Two-Stage Experimental Intelligent Dynamic Energy Management of Microgrid in Smart Cities based on Demand Response Programs and Energy Storage System Participation

Sepehrzad, Reza ; Hedayatnia, Atefeh ; Amohadi, Mahdi ; Ghafourian, Javid ; Al-Durra, Ahmed ; Anvari-Moghaddam, Amjad

Published in:
International Journal of Electrical Power & Energy Systems

DOI (link to publication from Publisher):
10.1016/j.ijepes.2023.109613

Publication date:
2024

Document Version
Publisher's PDF, also known as Version of record

Electrical Power and Energy Systems 155 (2024) 109613

Contents lists available at ScienceDirect

International Journal of Electrical Power and Energy Systems

journal homepage: www.elsevier.com/locate/ijepes

Two-Stage experimental intelligent dynamic energy management of microgrid in smart cities based on demand response programs and energy storage system participation

Reza Sepehrzad [a,*], Atefeh Hedayatnia [b], Mahdi Amohadi [c], Javid Ghafourian [d], Ahmed Al-Durra [e], Amjad Anvari-Moghaddam [f]

[a] Department of Electrical Engineering, Politecnico di Milano University, Milan, Italy
[b] Department of Electrical Engineering, Hamedan University of Technology, Hamedan, Iran
[c] Department of Electrical Engineering, Mohajer Technical University of Isfahan, Isfahan. Iran
[d] Department of Electrical Engineering, Iran University of Science and Technolog, Tehran, Iran
[e] Advanced Power & Energy Center, EECS Department, Khalifa University, Abu Dhabi, UAE
[f] Department of Energy (AAU Energy), Aalborg University, 9220 Aalborg, Denmark

ARTICLE INFO

Keywords:
Microgrid
Power and Energy Management
Voltage/Frequency Control
Smart Cities
Demand Response Program

ABSTRACT

Power variations due to uncertainties create fluctuations in voltage/frequency (V/F). Most critical microgrid's (MG) challenge in smart cities is V/F stability considering uncertainties in different operating conditions. This study proposes an energy management platform based on an intelligent probabilistic wavelet petri neuro-fuzzy inference algorithm (IPWPNFIA) to control the V/F index in the presence of renewable energy sources (RESs) and battery energy storage system (BESS) facing with various uncertainties. The suggested approach is programmed at two central and local controller stages based on the communication system and time-of-use demand response programs execution. The suggested approach is modeled by considering asymmetric membership functions based on the BESS optimal participation to control uncertainties caused by RESs, plug-and-play operations, and load fluctuations. The proposed platform's performance is verified and compared in different scenarios with different methods. The experimental setup and results are based on the rapid control prototyping of the micro-grid platform, MATLAB/Simulink and RT-LAB software, and hardware infrastructure such as the OPAL-RT (OP5600/OP8660) System. The most important highlights of this research are: fast dynamic response, real-time control based on real data, reducing the calculation time and burden based on learning algorithms, and the suitable coordination to adjust the protection equipment pick-up time.

1. Introduction

Environmental concerns caused by reduced fossil energy sources, increased greenhouse gas (GHG) emissions, and restructured traditional energy distribution systems have raised the microgrid (MG) idea. MG structure, relying on unique features, is an attractive answer to the challenges of the energy industry as well as environmental concerns [1,2]. MGs have been developed using two grid-connected and islanded operation modes, taking advantage of their potential and actual capacities in providing solutions appropriate to energy distribution system challenges and establishing a reliable and efficient RES-based integrated distribution system, including solar and wind power [3,4]. Numerous challenges influence MGs' performance and operation despite their numerous technical, economic, and environmental advantages. These include improved security, reliability, and resilience, reduced operation service and maintenance costs, and mitigated the GHG using RESs [5]. On the one hand, RESs' uncertainties, and MGs' complex security,

Abbreviations: AGF, Asymmetric Gaussian Function; AMI, Advanced Metering Infrastructure; ANN, Artificial Neural Network; BESS, Battery Energy Storage System; EV, Electric Vehicle; IPWPNFIA, Intelligent Probabilistic Wavelet Petri Neuro-Fuzzy Inference Algorithm; MG, Microgrid; MGCC, Micro-Grid Central Controller; MGLC, Micro-Grid Local Controller; OPF, Optimal Power Flow; PV, Photovoltaic Panel; PID, Proportional-Integral-Derivative; RES, Renewable Energy Source; RNN, Recurrent Neural Network; RCP-MG, Rapid Control Prototyping of the Micro-Grid; SOC, State of Charge; TOU-DRP, Time-of-Use Demand Response Program; V/F, Voltage/Frequency; WT, Wind Turbine.

* Corresponding author.
E-mail address: sepehrzad.reza@gmail.com (R. Sepehrzad).

https://doi.org/10.1016/j.ijepes.2023.109613
Received 25 May 2023; Received in revised form 9 October 2023; Accepted 23 October 2023
Available online 8 November 2023

Nomenclature

$PDF(P_{wind}), PDF(P_{solar})$ $PDF(f_{EV}^{AT}), PDF(f_{EV}^{DT})$ $PDF(f_D), PDF(P_{Load})$	Probability distribution function of different parameters
$\sigma_{wind}, \mu_{wind}$ $\sigma_{solar}, \mu_{solar}$ $\sigma_{EV}^{AT}, \mu_{EV}^{AT}$ $\sigma_{EV}^{DT}, \mu_{EV}^{DT}$ $\sigma_{Load}, \mu_{Load}$	Mean and standard deviation of Various parameters
$OMC_{MG,i}^{Grid}, OMC_{Disel}, OMC_{RES}, OMC_{BESS}$	Operation and maintenance cost ($/kWh)
$v_t, v_r, v_{cut-in}, v_{cut-out}, v_{wind}$	Instantaneous wind speed, rated wind speed. Cut-in speed, cut-out speed, wind speed (m/s)
P_{wind}	The wind power (kW)
P_{WT}, P_{WT-r}	The Wind turbine power, rated wind turbine power (kW)
P_{solar}, P_{PV}	The Solar power, PV power (kW)
$P_{BESS}^{i}(t)$	The BESS power (kW)
$P_{Load}^{DRP}(t)$	Load power based demand response programs (kW)
$P_{MG,i}^{Grid}(t)$	The power exchanged between the micro-grid and the main grid (kW)
$P_{Disel}^{i}(t)$	The power of diesel generators (kW)
$P_{MG,i}^{Net}(t)$	Net power of the micro-grid (kW)
$P_{RES}^{i}(t)$	Power of renewable energy sources (kW)
$P_{MG,i}^{Grid,Pre}(t), P_{MG,i}^{Grid,Err}(t)$	Predicted power and predicted power error exchanged between the micro-grid and the main grid (kW)
$P_{RES}^{i,Pre}(t), P_{RES}^{i,Err}(t)$	Predicted power and predicted power error of RES (kW)
$P_{BESS}^{i,Pre}(t), P_{BESS}^{i,Err}(t)$	Predicted power and predicted power error of BESS (kW)
$P_{Load}^{0}(t)$	The Initial load (kW)
$P_{Bat-EV}(t)$	The EV battery power (kW)
P_{Load}	The Load power (kW)
P_{ref}, P_{ins}	Reference active power, instantaneous active power (operation power) (kW)
D_i^0	The Initial power (kW)
∂D_i	Sensitivity of subscribers' demand to price changes. (kW/$)
Q_{ref}, Q_{ins}	Reference reactive power, instantaneous reactive power (operation power) (kVAR)
V_{ref}, V_{ins}	Reference voltage, instantaneous voltage (operating voltage) (kW)
V_{MPP}, V_{OC}	Maximum power point voltage and PV open circuit voltage (V)
V_r, f_r	Threshold V/F pick-up protection equipment (V, Hz)
f_{ref}, f_{ins}	Reference frequency, instantaneous frequency (operating) (Hz)
I_{MPP}, I_{SC}	Maximum power point current and PV short circuit current (A)
$i_{q-P}^{Operation}, i_{d-Q}^{Operation}$	Operational signals of converters (A)
T_m	Maximum pick-up time of protection equipment (s)
$T_{Operation}$	Pick-up time of protection equipment (s)
t_{ch}	The Charging time (h)
T_h	The Planning time horizon (h)
N	PV panel modules
k_v, k_i	The Voltage and current gain
k_{EV}^{AT}, k_{EV}^{DT}	The Standard deviation
d	The variance of the distribution (km)
$D_{Bat-\max}, D_{Bat-EV}$	Maximum distance traveled per charge, distance traveled per charge (km)
$b_{Bat-EV}^{ch}, b_{Bat-EV}^{dis}$	The Binary variables
$C_{BESS}(t)$	The BESS capacity (Ah)
s_{BESS}	The Self-discharge coefficient
DM_i	Decision making index
$\mathrm{EL}_{i,i}^{SE}, \mathrm{EL}_{i,j}^{ME}$	The Self and mutual elasticity
$\partial\delta_{i,j}$	The Price changes ($)
$\delta_{i,j}^{0}$	The Initial price ($)
η^{DRP}	Participation of loads in demand response programs (%)
$IO(i,j)$	Incentive offered ($)
$\sigma_{LU}(t)$	The Load uncertainty index
E^{absolute}	The Absolute error integral index
$\lvert e(t)\rvert$	The Absolute error
e	Error of reference values from instantaneous values (operating values)
$\widehat{e}_{Pre}$	Prediction error from actual values in each iteration I
$N_i^L(I)$	Neural networks in each layer
x_i^L	The Input to layer
y_i^L	The Output from layer
L	The Layer symbol
M_j^{L2}	Mean of asymmetric Gaussian function
M_{ik}^{L3}	Mean of Wavelet function
$d_{right-j}^{L2}, d_{left-j}^{L2}$	Right and left deviation of asymmetric Gaussian function
d_{ik}^{3}	Deviation of Wavelet function
$W_{ik}^{L3}(I)$	Wavelet function output
w_{ik}^{L3}	Weight of Wavelet function output
w_{jl}^{L4}	The weighted fuzzy rules layer
w_{lo}^{L5}	The weight of the defuzzification layer
Δw^L	Weight change index of each layer
w^L	Updated weight index of each layer
$\lambda_k^{L3}(I)$	Summation Wavelet function output
$T_s^{L3}(N)$	Transition state layer 3
f_{th}	Threshold Petri function.
a, b	Positive constants
k_1, k_2	Positive coefficients of protection
c_1, c_2	Shape and scale factors
V	Average actual and predicted error
$O.F$	The objective function
σ^L	Error index of each layer based on the propagated process
μ	The learning rate of each layer

reliability, and resilience metrics, and on the other hand, the launch of energy management systems (EMSs), the deployment of smart grid platforms, and complex big data analytics caused by multiple decision-making variables and linear/non-linear/randomized/probabilistic uncertainties are considered to be fundamental challenges facing the MG concept. The mentioned challenges face the EMS structure with significant changes. It can be mentioned that some challenges, such as evaluating big data and considering uncertainties, not only increase the dimensions of the energy management problem, but also make the EMS structure index more complex [6,7]. Therefore, researchers have conducted several studies leading to the establishment of integrated intelligent energy control and management systems based on various analytics, including V/F control, power control, demand response program (DRP) implementation, grid restoration, and BESS participation.

Numerous smart models and algorithms have been proposed to tackle MG challenges.

In [8], a bi-level MG energy control and management model to control MG power, voltage, and frequency metrics based on a model-based predictive control (MPC) algorithm at the primary level and an intelligent neural network (INN) algorithm at the secondary level is proposed. The proposed approach is modeled in a communication system context considering the uncertainties caused by communication system latency and load fluctuations. Although the suggested approach's performance was analyzed in different scenarios, the model was proposed without considering and modeling RES uncertainty. RES uncertainty modeling is of great importance because the uncertainty caused by RES leads to variations in MGs' net active and reactive powers. In [9], an energy management and control strategy for optimal and real-time operation of virtual power plants (VPPs) based on the MPC technique and feedback correction (FC) algorithm, aiming to minimize RESs' uncertainties and prediction error deviation is developed. The suggested approach's performance was verified in a real electric energy distribution grid based on minimum demand and supply errors. The main challenge of this study is the high computational time and failure to verify the MG performance stability based on advanced control theories, such as the Nyquist stability criterion, Root Locus method, and small-signal analysis. In [10], a multi-level MG power management and control strategy based on primary, secondary, and tertiary objectives is developed. The primary objectives include voltage quality improvement and V/F metric restoration. In secondary, V/F deviations of MG are minimized by determining the secondary controller coefficients through a distributed fuzzy controller (DFC). Tertiary objectives also manage the bidirectional power exchange control between the MG and the upstream grid. The suggested approach constructed an inflexible structure for subscribers' participation in the electricity market, regardless of energy storage systems (ESSs) and DRPs. The suggested approach was also based on low-uncertainty power supply sources, including fossil fuels-based distributed generations (DGs), and avoided using RES and its uncertainty modeling. The RES smart management strategy based on a hybrid artificial neural network-particle swarm optimization algorithm (ANN-PSO) method was proposed in [11] to minimize computing time and maximize flexibility. The optimization algorithm search space was programmed based on optimizing the nodes in the hidden layers and improving the training rate to minimize the computing time of the optimal power distribution in the MG configuration. The most prominent challenge of this research is the exponential increase of the processing operations due to the increase in the dimensions of the problem as well as considering a wide range of uncertainties. Therefore, with the significant increase in processing operations, the calculation time also increases significantly.

In [12], the MG performance by considering energy market interactions and proposed a bi-level pricing model based on estimation and reinforcement learning (RL) metrics to tackle the challenges of RESs' and time-varying uncertainties of energy carrier prices in the retail market using an ANN algorithm is investigated. In addition, in [13], also a distributed robust model predictive control (DRMPC) method in the MG islanded configuration, aiming to (1) establish an energy market based on energy market interactions and (2) minimize RESs' uncertainties is proposed. This study modeled RES probability behavior using an intelligent ANN (IANN) algorithm to minimize RESs' uncertainties and data prediction errors. Combining the stochastic processes and IANN algorithms improved the control models' performance. The most obvious challenge of the two mentioned researches is the low dynamic speed to respond to instantaneous fluctuations. In [14], a load control platform in residential MG and the participation of electric vehicle (EV) units in optimal power distribution based on stochastic Markov decision process (MDP), recurrent neural network (RNN) algorithm, and deep reinforcement learning (DRL) is presented. Control objectives are implemented in MGs based on time frames and in three primary, secondary, and tertiary control levels. In [15], a two-layer strategy for the optimal control and stability of MG voltage and minimizing the operational time of the suggested approach by considering active power generation sources, capacitor bank, and tap changer variations of transformers based on deep neural network (DNN) algorithm is developed. The suggested approach performance was evaluated in different scenarios regardless of the ESS and RES units and the uncertainties caused by them. In [16], an economic model for networked-microgrid primary and secondary frequency control based on a multi-agent DRL (MA-DRL) method is proposed. In the suggested approach, each DRL agent is responsible for controlling the generator power of ESS units. An offline training framework teaches the optimal frequency control strategy based on the soft actor-critic (SAC) algorithm. The suggested approach schedules each agent using its local and neighboring data. Hence, it is less precise than global variations in MG. In [17], the MG frequency control platform by combining DRL and multi-agent quantum machine learning (MAQML) based on intelligent data mining and feature extraction algorithms to tackle this challenge and increase precision is proposed. Although the suggested approach has a remarkable performance in frequency control, but the interference of the suggested approach with the protection equipment is considered the most prominent challenge of this research.

Uncertainties and probability patterns due to subscribers' behaviors and RESs affect MG's optimal and efficient operation. Power harvesting from RES is influenced by weather conditions and seasonal variations [18]. Therefore, the power harvested from RESs is highly uncertain and classified as stochastic sources. Power variations due to RESs' uncertainty negatively affect protection equipment operations and cause recurrent outages in power grids. Today, ESSs not only mitigate the effects of uncertainties in the real-time energy distribution systems and MGs, but the use of ESSs with DRPs has highlighted the role of subscribers in the energy market [19]. The use of DRP not only provides the framework for restructuring the electricity market but also demonstrates the critical role of subscribers in optimal power distribution by modifying the subscriber's load profile. The BESS is one of the most common storage system [20]. Due to the growing use of EVs in current grids, the BESS is considered one of the main constituents of EVs. Therefore, modeling and analyzing EVs' impact on power distribution grids is important [21]. EV units in power flow equations are considered loads or power suppliers. Since consumers' behavior has a probability pattern, it is essential to provide a control model based on uncertainties and the probability pattern of subscribers' behavior [22]. For instance, in [23], the EV battery charge management during grid congestion and peak load hours based on real-time mechanisms and fair and dynamic resource allocation is presented. This study developed optimal and hierarchical MG management using stochastic inputs, including RES uncertainties, the prediction model of connecting EVs to MGs, and EVs' charging status based on discrete-time Markov chain (DTMC).

In [24], a bi-level optimal distribution model in the integrated energy system (IES) and electric vehicle charging station (EVCS) by considering RES uncertainties and enhancing flexible load participation, aiming to balance energy supply and demand and increase customer satisfaction at an acceptable level to maximize subscribers' participation in the energy market and adjust subscribers' load profiles is proposed. This study presented DRP execution algorithms based on two dynamic mechanisms: Time-of-Use (TOU) pricing and real-time pricing (RTP). In addition, in [25], a resilient MG control model by considering EV participation in improving energy distribution in an islanded MG and implementing DRP to modify subscribers' load profiles and maximize their participation in energy distribution is also proposed. The research model involves the implementation of a hybrid dynamical system theory in which the continuous-time dynamics component is responsible for managing EVs' adjustable loads. On the other hand, discrete-time dynamics algorithms manage the shiftable loads. The suggested approach exhibits suitable performance under plug & play operating conditions and load fluctuations.

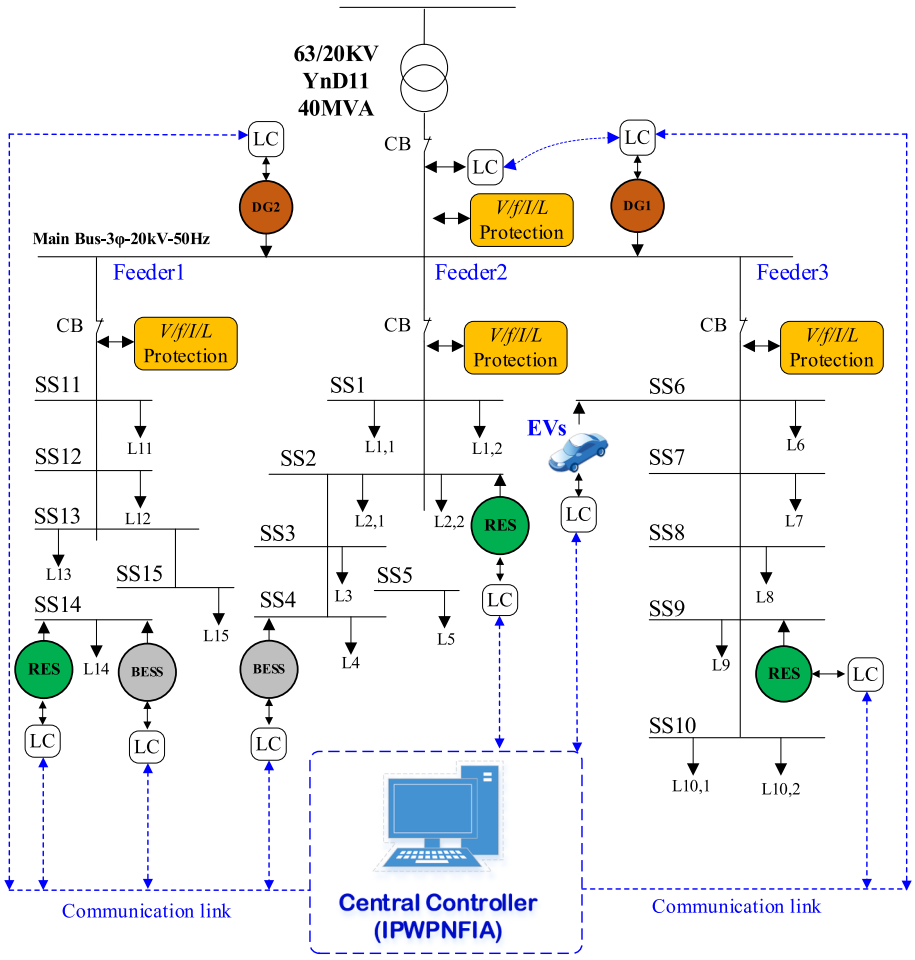

Fig. 1. The MG topology based on MGCC and MGLC in the context of the communication system.

1.1. Problem statement and research gap

According to the evaluation of previous research, the most obvious challenges of EMS in MG structure can be mentioned. Among the most obvious challenges of EMS are the evaluation of big data and various uncertainties. The assessment of big data and uncertainty not only complicates the structure of EMS, but also has a significant impact on processing operations, computation time, and load. One of the most important requirements of the EMS structure is the fast dynamic response in the face of instantaneous changes and oscillations. If the calculation time and burden in EMS are time-consuming and huge, not only the control approaches do not have a suitable dynamic response, but the efficiency of EMS in controlling instantaneous changes and oscillations decreases significantly. On the other hand, since EMSs are responsible for controlling normal transient events, therefore, the EMS structure must be designed in such a way that it has the necessary coordination with protection equipment that is responsible for handling unexpected transient events. Therefore, in this research, the proposed approach is presented by considering the properties of the data, as well as the classification of the data based on the uncertainty model, as well as using the multi-level intelligent method with an improved learning structure. In addition to handling a wide range of uncertainties and random variables, the proposed approach has high dynamic speed. Also, the proposed approach has a suitable coordination with protective equipment. Also, in this research, in order to evaluate and validate the simulation results, experimental results based on IEEE 644–2019 and IEEE 1159–2009 standards have been implemented in the structure of the current electrical distribution network (real grid) and its numerical results have been presented.

2. Research objectives and innovation

The MG model proposed in this study is real grid-based and is a portion of the electrical energy distribution network of Rajaee Port in Iran. The control models proposed in this study are analyzed and verified in the target grid, and the experimental results are also provided. As shown in Fig. 1, a portion of Rajaee Port's 16-bus electrical distribution grid is equipped with wind-solar RESs and the BESS. The proposed grid comprises a high voltage (HV) substation of 63/20 kV and 65 medium voltage (MV) substations of 20/04 kV.

The grid is connected to the controller and monitoring centers through the dispatching system and protection equipment, such as line, generator, feeder, voltage, and frequency protection (IEC60870-5–103,104) based on an optical fiber communication system supported by IEC61850 protocols. Each MV substation is abbreviated as the SS symbol. The power generation and ESS units are connected to the micro-grid central controller (MGCC) through the micro-grid local controller (MGLC). This portion of the distribution grid is utilized to supply power to the residential town located 3 km from the 63/20 kV substation. The proposed grid contains two diesel generators with a nominal power of 500 kW (SD500 | 15.2L | GENERAC model, each diesel can only be used with 85 % nominal power due to weather conditions and regional factors), a wind turbine (WT) with 110 kW power, a photovoltaic panel (PV) (Chroma 62150H-6005 model) with 110 kW power, and BESS set (Nissan Altra lithium-ion battery model) with 230 kWh power. In this grid, 30 % of the BESS power comprises the EV battery power and a load

set equal to 1400 kW with a 75 % simultaneity factor connected to the electric grid by advanced metering infrastructures (AMIs) based on the GPRS protocol.

This portion of the grid involves various uncertainties, including the disconnection of the diesel generator from the MGs, the uncertainty of RES power generation, and the islanding of this portion of the grid, leading to the instability of V/F metrics in the target MG. V/F instability is caused by variations in MG's net active and reactive power, activates V/F protection relays, and impairs MG operation under various uncertainties. The decrease in security and reliability indicators is caused by the failure to control uncertainties in the proposed grid. However, an intelligent control model can mitigate risks due to uncertainties significantly and avoid unnecessary protection equipment operation. Consistent with IEEE 644–2019 and IEEE 1159–2009 standards, V/F control requirements for MG operation are determined in two main grid-connected and islanded operation modes.

The main contribution of this study is to propose the IPWPNFIA considering asymmetric membership functions based on the BESS units participation to control RES uncertainties, monitor plug & play operation conditions in power generation units and load fluctuations with fast dynamic response, and mitigate transient risks in the power system. The proposed control algorithm considers the TOU-DRP metric to manage the BESS units' operations, including EV batteries, to control the power and V/F of MGs. The IPWPNFIA controller model is mainly based on data prediction and probability indicators. Therefore, by using probability tools such as probability distribution functions with normal distribution and their generalized types to model uncertainties caused by the RES and EVs and significantly minimize prediction errors. The decrease in data prediction error makes the proposed algorithm more accurate and reduces the computing time. Since the suggested approach is rule and knowledge-based, the IPWPNFIA controller minimizes the number of fuzzy function rules to reduce the computing time by taking advantage of the previous data-based training capability. The suggested approach was developed based on MGCC and MGLC configuration and communication infrastructure. MGLC provides MGCC with day-ahead power prediction using day-ahead algorithms. Based on the IPWPNFIA, MGCC also computes intelligent power distribution and adjustment of V/F metrics in MGs, making them available to MGLC converters again. Since the suggested approach was implemented in a portion of the electrical energy distribution grid of Rajaee Port in Iran (a real small-scale MG), the performance of the suggested approach and IPWPNFIA controller is verified through different scenarios, the experimental results is presented, and the performance is also compared with other general and intelligent methods, e.g., PID and ANN. The experimental setup was designed and proposed using the RCP-MG platform, MATLAB/Simulink and RT-LAB software, and hardware infrastructures, e.g., OPAL-RT hardware (OP5600 and OP8660) Lab-Volt Electromechanical Training System.

The most important highlights of this research are: Fast dynamic response, real-time control based on real data, reducing the calculation time and burden based on learning algorithms, as well as the suitable coordination to adjust the protection equipment pick-up time.

2.1. Main contribution and objectives

The **main contribution** of the study can be summarized as follows:

1. Propose a multi-level V/F metric control model based on the IPWPNFIA and the optimal BESS participation, aiming to mitigate RES uncertainties, control plug & play operating conditions, and improve the performance of protection relays when facing uncertainties.
2. Facilitate the setting of control metrics and minimize the deviation error of active/reactive power from reference point values to provide a fast dynamic response, mitigate the power system's transient risks, and maximize RES and BESS penetration in real-world power grids.
3. Provide the proposed controller model's experimental results by considering standard protection equipment metrics, adjusting the protection equipment pick-up time, and controlling the V/F deviation metric in a real-time framework.

The rest of the paper is organized as follows: In section 2, the probability model of the MG equipment and the power exchange equations between the MG and the main grid are presented. In the section 3, the problem solving algorithm based on the IPWPNFIA method is presented. The section 4 presents simulation and experimental results, and the section 5 presents conclusion, challenges, and future work.

3. MG topology and equipment

In this section, the MG topology based on the presence of RES, BESS units, MG power exchange equations, and MGCC and MGLC controllers are expressed.

3.1. RES uncertainty model

As stated, because the power generation by the RES is dependent on weather conditions, therefore, power extraction from the RES has a probability and random pattern. To model the power generation of PVs, the beta probability distribution function model is used, and for the WT, the Weibull probability distribution function is used. In addition to the high potential of solar radiation, the geographical location of Iran's Rajaee port also benefits from the high potential of wind power [26].

$$PDF(P_{wind}) = \frac{c_1}{c_2}\left(\frac{v_{wind}}{c_2}\right)^{c_1-1} e^{\left[-\left(\frac{v_{wind}}{c_2}\right)^{c_1}\right]} \Rightarrow \begin{cases} c_1 = \left(\dfrac{\sigma_{wind}}{\mu_{wind}}\right)^{-1.086} \\ c_2 = \dfrac{\mu_{wind}}{\Gamma(1+\frac{1}{c_1})} \end{cases} \quad (1)$$

$$P_{WT} = \begin{cases} 0, \ 0 \le v_r < v_{cut-in}, v_r \ge v_{cut-out} \\ P_{WT-n}\dfrac{v_r - v_{cut-in}}{v_n - v_{cut-in}}, v_{cut-in} \le v_r < v_n, t > 0 \\ P_{WT-n}, v_n \le v_r < v_{cut-out} \end{cases} \quad (2)$$

$$\begin{cases} PDF(P_{solar}) = \dfrac{\Gamma(c_1+c_2).(1-P_{solar})^{c_2-1}.(P_{solar})^{c_1-1}}{\Gamma(c_1)+\Gamma(c_2)} \\ c_1 = \dfrac{\mu_{solar}.c_2}{1-\mu_{solar}} \\ c_2 = \left(\dfrac{\mu_{solar}.(1-\mu_{solar}^2)-\sigma_{solar}^2}{\sigma_{solar}^2}\right), c_1, c_2 > 0 \end{cases} \quad (3)$$

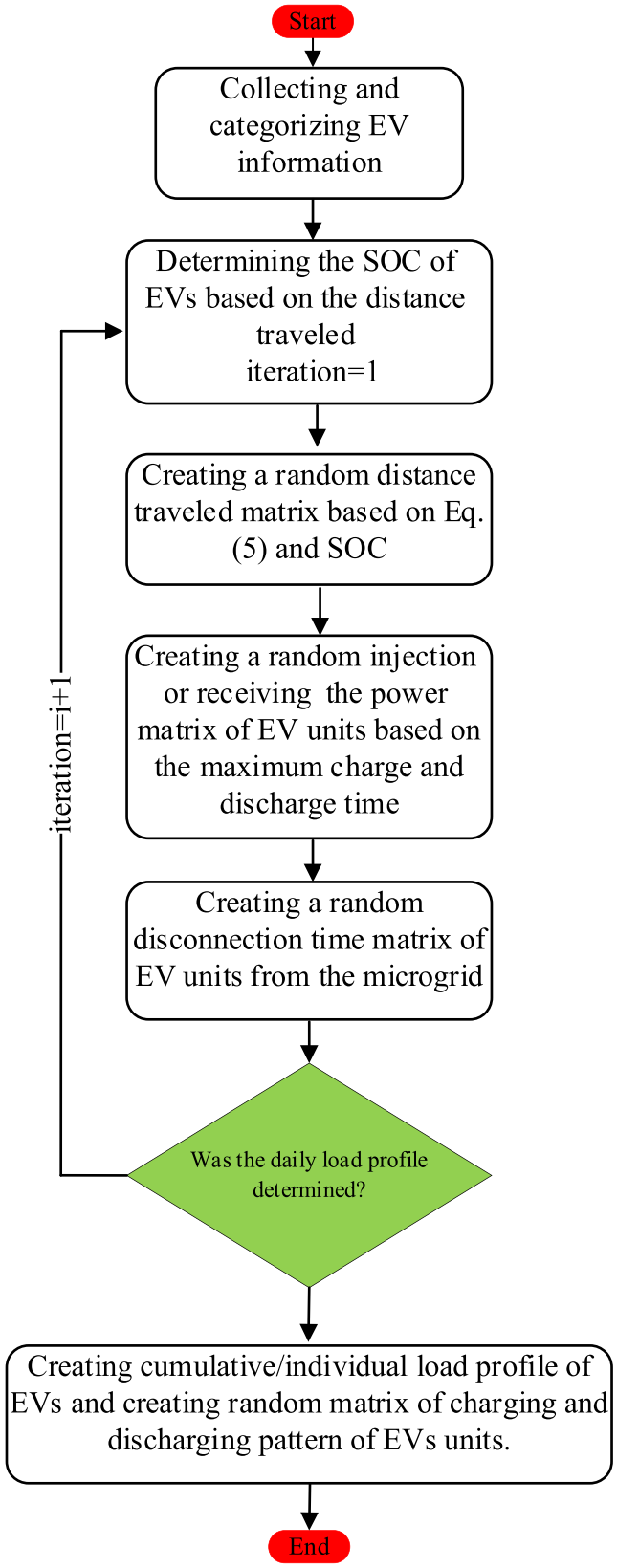

Fig. 2. Determination of EV units load profile.

$$P_{PV} = N.\frac{(V_{MPP}.I_{MPP}).(V_{OC} - k_v T_{PV}).([I_{SC} + k_i(T_{PV} - 25)])}{V_{OC}.I_{SC}}\Bigg|_{T_{PV}=T_{Amb}+\frac{P_{Rad}(T_{nom}-20)}{0.8}} \tag{4}$$

3.2. EV units uncertainty model

In power flow equations, EV units are considered either as electric load or as power supplier. Considering that the consumption pattern of subscribers has a random process, therefore, the use of probability models describes the consumption profile of EV units more accurately. In this section, the equations of the EV unit random process based on the Weibull normal distribution function and generalized types are presented in three categories in order to reduce the data estimation error [26,27]. The first category is when the EV unit is connected to the MG and either injects power into the grid or receives power from the grid. The second category is when the EV unit is separated from the MG and the third category shows the distance traveled by each EV unit along with the batteries state of charge (SOC_{Bat}). Eqs. (5) to (7) describe the EV unit behavior. Eq. (8) also expresses the EV unit power.

$$PDF(f_{EV}^{AT}) = \frac{e^{-\left(1+\frac{k_{EV}^{AT}.(d-\mu_{EV}^{AT})}{\sigma_{EV}^{AT}}\right)^{-\left(\frac{1}{k_{EV}^{AT}}\right)}}.\left(1+\frac{k_{EV}^{AT}.(d-\mu_{EV}^{AT})}{\sigma_{EV}^{AT}}\right)^{-\left(1+\frac{1}{k_{EV}^{AT}}\right)}}{\sigma_{EV}^{AT}} \tag{5}$$

$$PDF(f_{EV}^{DT}) = \frac{e^{-\left(1+\frac{k_{EV}^{DT}.(d-\mu_{EV}^{DT})}{\sigma_{EV}^{DT}}\right)^{-\left(\frac{1}{k_{EV}^{DT}}\right)}}.\left(1+\frac{k_{EV}^{DT}.(d-\mu_{EV}^{DT})}{\sigma_{EV}^{DT}}\right)^{-\left(1+\frac{1}{k_{EV}^{DT}}\right)}}{\sigma_{EV}^{DT}} \tag{6}$$

$$\begin{cases} PDF(f_D) = \dfrac{c_2.e^{-\left(\frac{t}{c_1}\right)^{c_2}}.\left(\frac{t}{c_1}\right)^{(c_2-1)}}{c_1}, t > 0 \\ SOC(P_{Bat-EV}) = \left(\dfrac{D_{Bat-\max} - D_{Bat-EV}}{D_{Bat-\max}}\right).100 \end{cases} \tag{7}$$

$$P_{Bat-EV}(t) = \begin{cases} P_{Bat-EV}^{\max}\left(1 - e^{\left[\frac{-(52.89)}{\tau_{ch}}\right]}\right),\ 0 < t \le t_{ch} \\ P_{Bat-EV}^{\max}\left(\dfrac{5 - t_{ch}}{5}\right),\ t_{ch} < t \le 5 \\ 0,\ t > 5 \\ b_{Bat-EV}^{ch} + b_{Bat-EV}^{dis} = 1, \forall t b_{Bat-EV}^{ch}, b_{Bat-EV}^{dis} \in \{0,1\} \\ P_{Bat-EV}^{\min} \le P_{Bat-EV}(t) \le P_{Bat-EV}^{\max} \Rightarrow P_{Bat-EV}^{\min} = (1 - DOD).P_{Bat-EV}^{\max} \end{cases} \tag{8}$$

In this study, the characteristics of the battery are according to the specification of "Nissan Altra lithium-ion battery" which is $P_{Bat-EV}^{\max} = 6.5kW$. The algorithm for determining the EV units load profile is shown in Fig. 2.

3.3. Load uncertainty model

Consumption loads profiles have a random process pattern because they are based on the random behavior of subscribers. Modeling of loads based on normal probability distribution function are described [26,27].

$$PDF(P_{Load}) = \frac{e^{\left[-\left(\frac{1-\mu_{Load}}{\sqrt{2}.\sigma_{Load}}\right)^2\right]}}{\sigma_{Load}\sqrt{2\pi}}, t > 0 \tag{9}$$

3.4. Power exchange model

The power exchange model is determined based on the net power of MG. The power exchange equations are [27]:

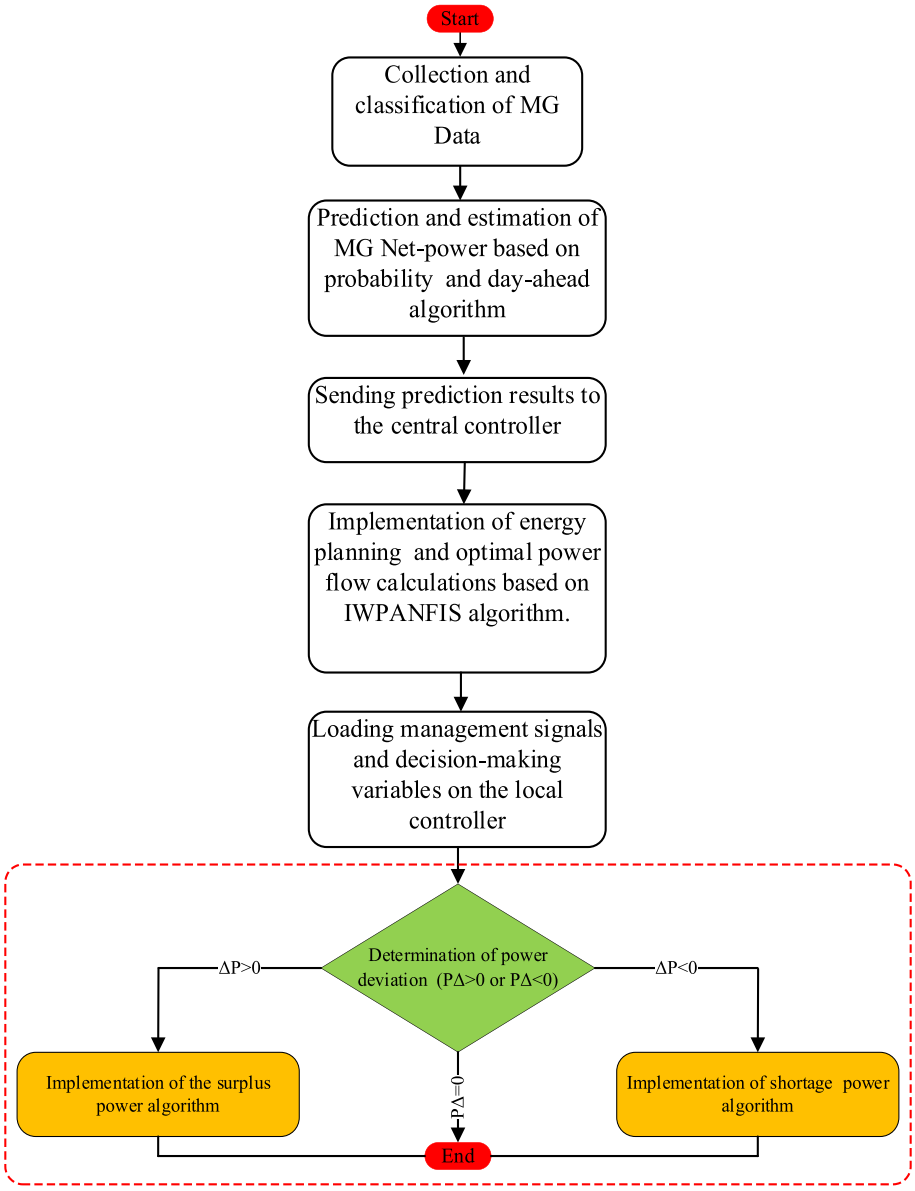

Fig. 3. Power exchange flowchart based on MGLC and MGCC.

$$C_{BESS}(t+1) = t.P^{i}_{BESS}(t) + s_{BESS}.C_{BESS}(t) \quad (9)$$

$$\pm P^{i}_{BESS}(t+1) = \pm DM_i.\left(\begin{array}{l}\sum_{i=1}^{N_i} P^{Grid}_{MG,i}(t) + \sum_{i=1}^{4} P^{i}_{Disel}(t) \\ + \sum_{i=1}^{N_{WT,i}} P^{i}_{WT}(t) + \sum_{i=1}^{N_{PV,i}} P^{i}_{PV}(t)\end{array}\right) - \left(\sum_{t=1}^{24} P^{DRP}_{Load}(t)\right) \quad (10)$$

Eq. (10) shows the amount of power stored in the battery based on the BESS capacity and the self-discharge rate at time *t*. Eq. (11) describes the battery power based on the generation and consumption powers in the MG. The MG generally have either surplus power or shortage power. The MGCC is responsible for controlling and managing optimal power distribution by receiving information from the MGLC that is planned based on the day ahead power prediction algorithms.

3.4.1. Power exchange model in MGCC

Because in MGs, different equipment with linear/non-linear or probabilistic characteristics are used, various uncertainties are effective on the performance and operation of MGs. In this study, the MGLC based on sampling and implementation of day-ahead power estimation algorithms are planned. The power prediction data in the MGLC is provided to MGCC using the communication system. The MGCC also performs planning and optimal power flow (OPF) calculations according to MGLC information and reloads the control results to MGLC [28,29]. The following equations describe the MGCC power exchange.

$$\left\{\begin{array}{l} P^{Net}_{MG,i} = DM_i.\left(\sum_{i=1}^{N_i} P^{Grid}_{MG,i}(t) + \sum_{i=1}^{4} P^{i}_{Disel}(t) + \sum_{i=1}^{N_{WT,i}} P^{i}_{WT}(t) + \sum_{i=1}^{N_{PV,i}} P^{i}_{PV}(t)\right) \\ \pm\left(\sum_{t=1} P^{i}_{BESS}(t)\right) - \left(\sum_{t=1}^{24} P^{DRP}_{Load}(t)\right), i \\ = 1, 2, \ldots, N \end{array}\right. \quad (12)$$

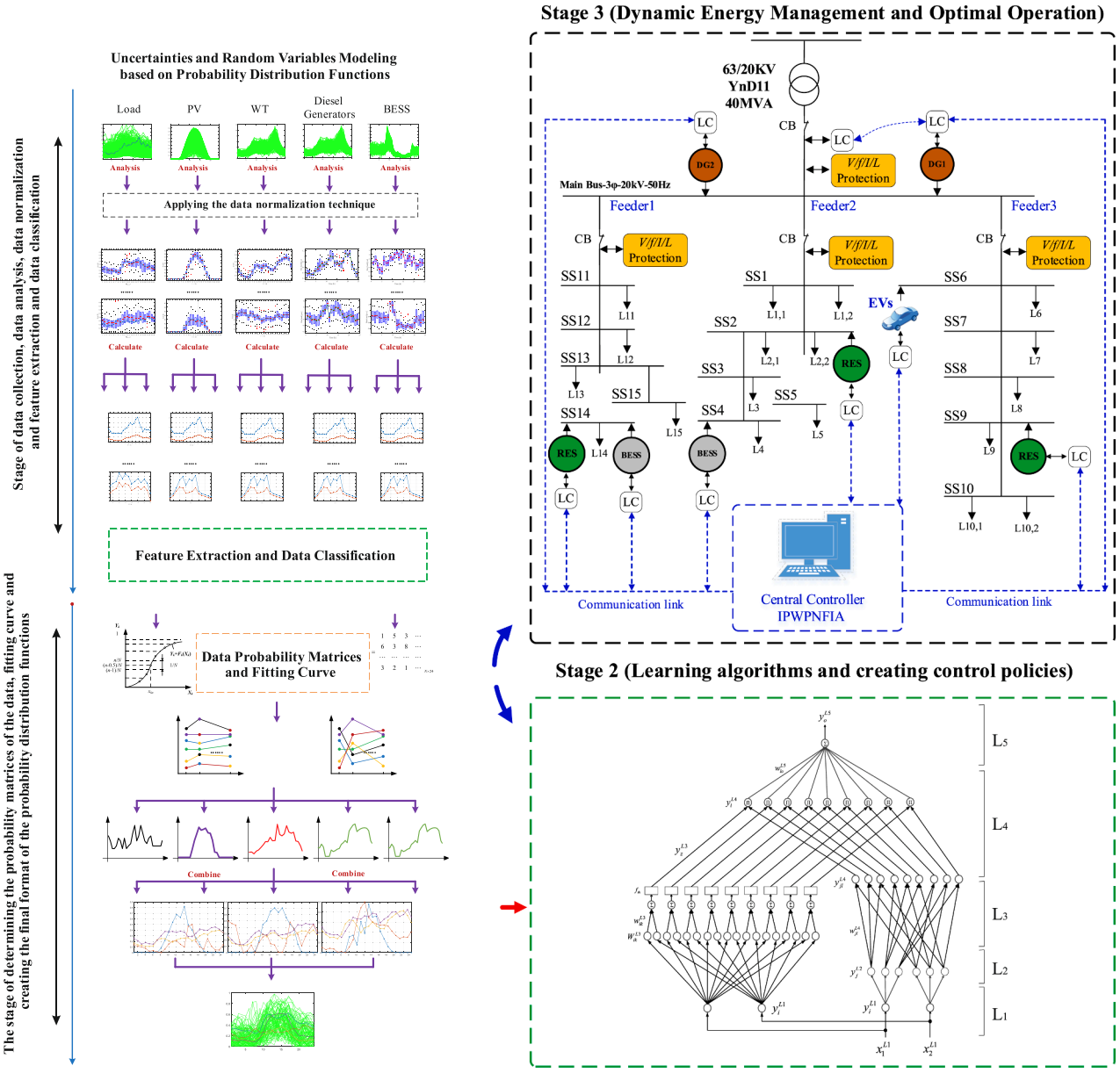

Fig. 4. Proposed algorithm.

$$f(\text{Receive the power shortage signal}) \Rightarrow \begin{cases} P^{Grid}_{MG,i}(t) > 0 \\ P^{i}_{BESS}(t) > 0 \end{cases}$$
$$if(\text{Receive the power surplus signal}) \Rightarrow \begin{cases} P^{Grid}_{MG,i}(t) < 0 \\ P^{i}_{BESS}(t) < 0 \end{cases} \quad (13)$$
$$P^{Grid-\min}_{MG,i}(t) \le P^{Grid}_{MG,i}(t) \le P^{Grid-\max}_{MG,i}(t), i = 1, 2, ..., N$$

Eq. (12) and Eq. (13) shows the net power of MG and the components affecting it. If the MGCC receives the shortage power signal, it schedules the operation of the MG based on the power received from the upstream grid and the power stored in the BESS. If the surplus power signal is received, MG operation is planned based on power storage in BESS units and sending power to the upstream network. The performance algorithm of MGCC is shown in Fig. 3.

3.4.2. Shortage power model in MGLC

The shortage power equations when the net power of MG is negative are as follows.

$$\min_{P^{Net}_{MG,i}(t,...,t+T_h-1)} \sum_{n=0}^{T_h-1} f(P^{Net}_{MG,i}(t+1)) \quad (14)$$

$$f(P^{Net}_{MG,i}(t+1)) = \left(\left(OMC^{Grid}_{MG,i}.P^{Grid}_{MG,i}(t)\right) + \left(OMC_{Disel}.P^{i}_{Disel}(t)\right) + \left(OMC_{RES}.P^{i}_{RES}(t)\right) + \left(OMC_{BESS}.P^{i}_{BESS}(t)\right)\right) \quad (15)$$

$$s.tC_{BESS}(t+1+n) = t.P^{i}_{BESS}(t+1) + s_{BESS}.C_{BESS}(t+1) \quad (16)$$

$$\pm P^{i}_{BESS}(t+1+n) = \pm DM_i.\left(\sum_{i=1}^{N_i} P^{Grid}_{MG,i}(t+1) + \sum_{i=1}^{4} P^{i}_{Disel}(t+1) + \sum_{i=1}^{N_{WT,i}} P^{i}_{WT}(t+1) + \sum_{i=1}^{N_{PV,i}} P^{i}_{PV}(t+1)\right) - \left(\sum_{t=1}^{24} P^{DRP}_{Load}(t+1)\right) \quad (17)$$

$$P_{MG,i}^{Grid}(t+1) = P_{MG,i}^{Grid,Pre}(t) + P_{MG,i}^{Grid,Err}(t) \tag{18}$$

$$P_{RES}^{i}(t+1) = P_{RES}^{i,Pre}(t) + P_{RES}^{i,Err}(t) \tag{19}$$

$$P_{BESS}^{i}(t+1) = P_{BESS}^{i,Pre}(t) + P_{BESS}^{i,Err}(t) \tag{20}$$

$$C_{BESS}^{\min} \le C_{BESS}(t+1) \le C_{BESS}^{\max},\ \mathrm{t} = 1, ..., T_h \tag{21}$$

$$P_{Load,i}^{DRP-\min} \le P_{Load}^{DRP}(t+1) \le P_{Load,i}^{DRP-\max},\ \mathrm{t} = 1, ..., T_h \tag{22}$$

Eq. (14) and Eq. (15) show the minimization of MG cost function during shortage power. Eq. (16) and Eq. (17) show the amount of power stored in the BESS unit during shortage power. Eqs. (18) to (20) show the MG operating power based on power prediction and prediction error caused by power uncertainties for the main grid, RES units and BESS units. Eq. (21) and Eq. (22) also show the BESS storage volume constraints and power consumption constraints.

3.4.3. Surplus power model in MGLC

The surplus power equations when the net power of MG is positive are as follows:

$$\min_{P_{MG,i}^{Net}(t,\ldots,t+T_h-1)} \sum_{n=0}^{T_h-1} f(P_{MG,i}^{Net}(t+1)) \tag{23}$$

$$f(P_{MG,i}^{Net}(t+1)) = \left(\left(OMC_{Disel}.P_{Disel}^{i}(t)\right) + \left(OMC_{RES}.P_{RES}^{i}(t)\right) + \left(OMC_{BESS}.P_{BESS}^{i}(t)\right)\right) \tag{24}$$

$$s.tC_{BESS}(\mathrm{t}\ +\ 1\ +\ \mathrm{n})\ =\ \mathrm{t.}\ \mathrm{P}_{BESS}^{i}(\mathrm{t}\ +\ 1) + s_{BESS}.C_{BESS}(\mathrm{t}\ +\ 1) \tag{25}$$

$$\pm \mathrm{P}_{BESS}^{i}(\mathrm{t}\ +\ 1\ +\ \mathrm{n}) = \pm DM_i.\left(\sum_{i=1}^{4} P_{Disel}^{i}(t+1) + \sum_{i=1}^{N_{WT,i}} P_{WT}^{i}(t+1) + \sum_{i=1}^{N_{PV,i}} P_{PV}^{i}(t+1)\right) - \left(\sum_{t=1}^{24} P_{Load}^{DRP}(t+1)\right) \tag{26}$$

(16)*to*(19)

The mentioned equations are the same as the shortage power equations, with the difference that in the condition of surplus power, the equations related to the upstream grid power are removed from the surplus power equations and while the rest of the formulation unchanged.

3.5. Load profile modification based on TOU-DRP and price elasticity model

In the proposed network, because the subscribers are equipped with advanced metering infrastructure (AMI) equipment based on the GPRS protocol, therefore, the TOU-DRP algorithm of the proposed micro-grid can be implemented [18,19]. Implementation of TOU-DRP algorithm based on price elasticity theory is presented. Price elasticity changes the subscriber consumption pattern based on price changes. Subscribers show two reactions to price changes. The first reaction is when subscribers are not able to transfer part of the load (such as lighting load) to other hours. This reaction shows negative elasticity and is known as self-elasticity. The second reaction is when subscribers change their consumption hours due to price changes and transfer part of their load to other hours [20]. This reaction shows positive elasticity or mutual elasticity. Eq. (27) describes self and mutual elasticity. Eq. (28) also shows the change of consumption pattern based on the TOU-DRP execution. Eq. (28) shows that not only the subscriber's load are not reduced, but the consumption time is simply transferred to other hours. It also shows the lack of increase in the price of subscribers' bills after the implementation of the TOU-DRP algorithm. Eq. (29) also shows the changes of the load curve compared to the initial conditions.

$$\mathrm{EL} = \begin{cases} \mathrm{EL}_{i,i}^{SE} = \dfrac{\delta_i^0}{D_i^0}.\dfrac{\partial D_i}{\partial \delta_i} \\ \mathrm{EL}_{i,j}^{ME} = \dfrac{\delta_j^0}{D_i^0}.\dfrac{\partial D_i}{\partial \delta_j} \end{cases} \tag{27}$$

$$P_{Load}^{DRP}(t) = \left\{ \eta^{DRP}.P_{Load}^{0}(t).\left(1 + \frac{\mathrm{EL}_{i,i}^{SE}.\left(\delta_i - \delta_i^0 + IO(i)\right)}{\delta_i^0} + \sum_{j=1, j\neq i}^{24} \frac{\mathrm{EL}_{i,j}^{ME}.\left(\delta_j - \delta_j^0 + IO(j)\right)}{\delta_j^0} \right) + \mathrm{EL}_{i,i}^{SE}.(P_{Load}^{0}(t)).(1+\sigma_{LU}(t)) \right\}, t > 0 \tag{28}$$

$$\Delta P_{Load}(t) = \eta^{DRP}.P_{Load}^{0}(t) - P_{Load}^{DRP}(t) \tag{29}$$

4. Control algorithm modeling and problem solving model

The V/F stability of power systems is of great importance, especially in the presence of various linear, non-linear and random equipment. Accurate control of power fluctuations in power systems results in the V/F control. Considering that the power extraction from the RES is based on random and probability variables, therefore, the RES penetration in current networks faces the challenge of V/F control. The use of intelligent control algorithm based on random variables is a suitable solution to meet the challenge of the power system's V/F control in the presence of RES. In the following, the IPWPNFIA model is presented. According to Fig. 4, the proposed approach is presented in three stages. Stage 1 includes data modeling and random variables based on probability distribution functions. Stage 2 includes learning algorithms and creating control policies for execution in the MG structure. Stage 3 also includes the execution of dynamic energy management and optimal operation in

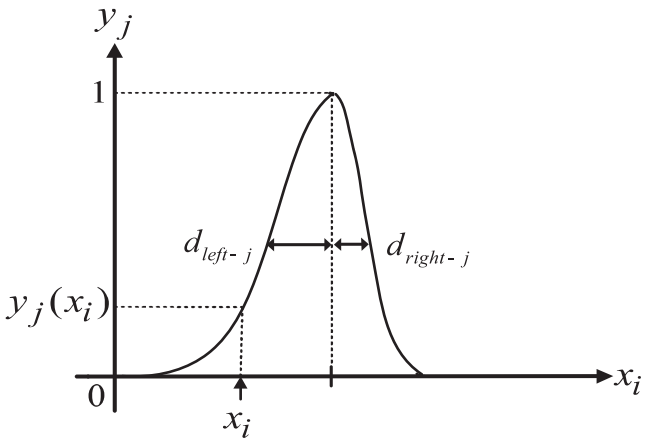

Fig. 5. AGF curve based on IPWPNFIA structure.

the MG structure. Stage 1 is divided into two parts. In the first part, the collected data are analyzed to determine the characteristics of the data. The most important data are load information, RERs, BESS and EVs, as well as diesel generators. Then, using data normalization technique and feature extraction, the data are classified into different categories. Then, in the second part, the data probability matrix is created based on probability distribution functions. Using the probability data matrix, the probability curve of the data is drawn. Then, using the curve fitting technique, the best curve based on the behavior of the data is created. Finally, the final format of data probability distribution functions based on the behavior and characteristics of each data is generated and classified. The results obtained in stage 1 are provided to stage 2 as input data. In stage 2, control policies and energy management signals are created using IPWPNFIA, and policies created in multiple episodes are trained using The Online Back-propagation Learning Algorithm. The IPWPNFIA model and The Online Back-propagation Learning Algorithm have a multi-level structure that makes it possible to avoid unnecessary and repetitive episodes and to perform processing operations in a shorter time. Therefore, this multi-level structure, in addition to reducing the computation burden and time, also reduces the memory capacity and processing operations and turns the serial processing operations into parallel processing operations to avoid unnecessary and repetitive processes. In stage 3 and after processing the data and creating control algorithms and energy management signals, the control policies are provided to the MGCC unit to execute dynamic energy management and optimal operation in the MG structure. According to the flowchart presented in Fig. 3, the MGCC unit provides the operating signal to various equipment in the MG in the context of the communication system, according to the conditions of surplus or shortage power. As long as there are no changes in the operation of MG, the control policies will remain according to the previous policies. If there are any changes in the operation, the MGCC unit again provides new control policies based on the new operation conditions, relying on the IPWPNFIA model and The Online Back-propagation Learning Algorithm to the MGLC units.

4.1. The IPWPNFIA model

According to Fig. 4 (stage 2), the IPWPNFIA is designed and modeled in 5 layers, including input layer (L1), membership functions layer (L2), Wavelet/Petri layer (L3), rule layer (L4) and output layer (L5). Because the structure of the suggested approach is modeled based on learning algorithms, therefore, in order to create a stable and robust platform, real-time control structure and the online back-propagation learning algorithm have been used in the suggested approach [30]. The proposed learning algorithm is not only used in the deep learning artificial neural networks algorithm, with more than one hidden layer to calculate the weight gradient more accurately, but also, this method often provides reduced gradient calculations of the objective function by optimizing the learning algorithm and stabilizing the weight of the neurons [31]. This algorithm is also used for feed-forward neural networks that require supervised learning [32]. The online back-propagation learning algorithm is also presented in 4 layers, which are membership functions layer (L2), Wavelet/Petri layer (L3), rules layer (L4) and outputs layer (L5). In the following, according to Fig. 4 (stage 2), the structure of the suggested approach is expressed in different layers.

Layer 1: Layer 1 includes inputs and outputs of neurons. In the proposed algorithm, the inputs include active and reactive power changes. Changes in active and reactive power cause changes in V/F. Therefore, in this study, 5 error variables are defined, which are:

$$\begin{aligned} e_1(I) &= e_P(I) = P_{ref} - P_{ins}(I) \\ e_1(I) &= e_Q(I) = Q_{ref} - Q_{ins}(I) \\ e_1(I) &= e_V(I) = V_{ref} - V_{ins}(I) \\ e_1(I) &= e_f(I) = f_{ref} - f_{ins}(I) \\ e_2(I) &= \widehat{e}_{Pre}(I) \end{aligned} \tag{30}$$

Which e indicates the error of the reference values from the instantaneous values (operation values) and $\widehat{e}$ indicates the prediction error from the actual values in each algorithm iteration I. Therefore, the first layer can be defined based on inputs and outputs as follows:

$$L_1 \begin{cases} N_i^{L1}(I) = x_i^{L1} \\ y_i^{L1} = f_i^{L1}(N_i^{L1}(I)) = N_i^{L1}(I), \ \mathrm{i} = 1,2 \end{cases} \tag{31}$$

Layer 2 (probability layer): According to Fig. 5, by using Asymmetric Gaussian Function (AGF), the structure of the second layer can be described based on each neuron that represents the membership functions. Therefore, the equations and output of layer 2 are:

$$L_2 \begin{cases} N_j^{L2}(I) = \begin{cases} -\dfrac{\left(x_i^{L2} - M_j^{L2}\right)^2}{\left(d_{left-j}^{L2}\right)^2}, & -\infty < x_i^{L2} < M_j \\ -\dfrac{\left(x_i^{L2} - M_j^{L2}\right)^2}{\left(d_{right-j}^{L2}\right)^2}, & \mathrm{M}_j < x_i^{L2} < +\infty \end{cases} \\ y_j^{L2} = f_j^{L2}(N_j^{L2}(I)) = e^{\left(N_j^{L2}(I)\right)}, \ \mathrm{j} = 1,2,..,6 \end{cases} \tag{32}$$

Layer 3: Layer 3 equations based on Wavelet/Petri function are provided. Therefore, the Wavelet/Petri output function based on the I_{th} neuron are:

$$Waveletfunction \begin{cases} W_{ik}^{L3}(I) = \dfrac{\left[1 - \dfrac{\left(x_i^{L1}(I) - M_{ik}^{L3}\right)^2}{\left(d_{ik}^3\right)^2}\right].\mathrm{e}^{\left[-\frac{\left(x_i^{L1}(I) - M_{ik}^{L3}\right)^2}{2\left(d_{ik}^3\right)^2}\right]}}{\sqrt{\left|d_{ik}^3\right|}}, \mathrm{k} = 1,2,...,9 \\ \lambda_k^{L3}(I) = \sum w_{ik}^{L3}.W_{ik}^{L3}(x) \end{cases} \tag{33}$$

$$Petrifunction \begin{cases} T_s^{L3}(N) - \begin{cases} 1, \lambda_k^{L3}(I) \geq f_{th} \\ 0, \lambda_k^{L3}(I) \leq f_{th} \end{cases}, \ \mathrm{th} = 1,2,...,9 \\ f_{th} = \left.\dfrac{a.\mathrm{e}^{(-b.V)}}{1 + \mathrm{e}^{(-b.V)}}\right|_{V = \frac{(e+\widehat{e})}{2}} \end{cases} \tag{34}$$

According to the equations of Wavelet/Petri layer, the equations of layer 3 can be described.

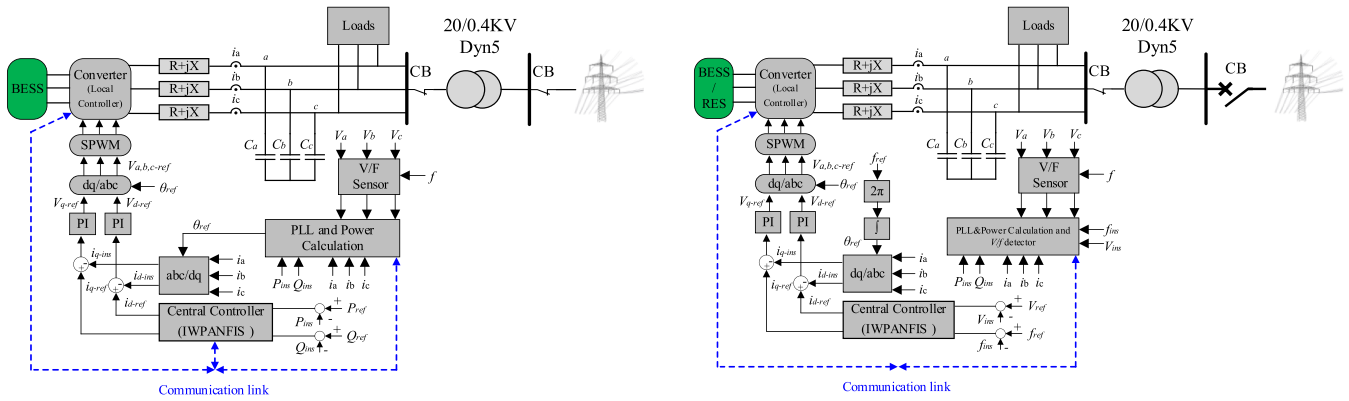

Fig. 6. Control structure based on IPWPNFIA. (a) The BESS unit power control in grid connection mode. (b) The BESS unit power control structure in islanded mode and the RES unit power control structure in grid connection and islanded modes.

$$L_4\begin{cases} N_z^{L3}(I)=\begin{cases}\lambda_k^3(I),\ \mathrm{T}_s^{L3}(I)=1\\ 0,\ \mathrm{T}_s^{L3}(I)=0\end{cases} \\ y_z^{L3}=f_z^{L3}(N_z^{L3}(I))=\left(N_z^{L3}(I)\right),\ z=1,2,..,9\end{cases} \tag{35}$$

Layer 4: This layer includes fuzzy rules and membership functions in the second layer. Fuzzy rules and membership functions are categorized and presented as normalized weights [33]. In this layer, the inference results from the fuzzy rules and membership functions are formed until in the 5th layer, the defuzzification operator is implemented and the final results are presented.

$$L_4\begin{cases} y_{jl}^{L4}=\prod_j w_{jl}^{L4}.y_j^{L2},\ 1=1,2,..,9 \\ N_l^{L4}(I)=y_{jl}^{L4}.y_z^{L3} \\ y_l^{L4}(I)=f_l^{L4}(N_l^{L4}(I))=\left(N_l^{L4}(I)\right)\end{cases} \tag{36}$$

Layer 5: In this layer, the defuzzification operator is activated and the output results of the IPWPNFIA are produced. The equations of this layer are:

$$L_5\begin{cases} N_o^{L5}(I)=\sum_{l=1} w_{lo}^{L5}.y_l^{L4}(I) \\ y_o^{L5}(I)=f_o^{L5}(N_o^{L5}(I))=\left(N_o^{L5}(I)\right),\begin{cases} y_o^{L5}(I)=i_{q-P}^{Operation} \\ y_o^{L5}(I)=i_{d-Q}^{Operation}\end{cases}\end{cases} \tag{37}$$

The results obtained from this layer include the control signals of the converters. Therefore, the active and reactive power controller currents of the converters are calculated and then sent to each converter.

4.2. The online back-propagation learning algorithm model

As stated, in order to create a stable and powerful platform, real-time control structure and online back-propagation learning algorithm have been used in the suggested approach. The online back-propagation learning algorithm is also presented in 4 layers, which are membership functions layer (L2), Wavelet/Petri layer (L3), rules layer (L4) and outputs layer (L5). If the objective function (O.F) in the modeling of the learning algorithm includes the decrease of the operating power error (Instantaneous powers) compared to the MG reference power, then the equations of the online back-propagation learning algorithm can be presented as follows:

$$O.F=\begin{cases}\frac{1}{2}\left(P_{ref}-P_{ins}\right)=\frac{1}{2}e_P(I)^2 \\ \frac{1}{2}\left(Q_{ref}-Q_{ins}\right)=\frac{1}{2}e_Q(I)^2\end{cases} \tag{38}$$

Eq. (38) shows the power error tracking in the learning algorithm. The error tracking operator tends the active and reactive power error to zero. Therefore, the error index and normalized weight update between layer 5 and 4 based on the propagation process and learning rate in layer 5 are:

$$Error_{L_5}\Rightarrow\sigma_o^{L5}=-\frac{\partial(O.F)}{\partial y_o^{L5}(I)}=-\frac{\partial(O.F)}{\partial P_{ins}}.\frac{\partial P_{ins}}{\partial y_o^{L5}(I)} \tag{39}$$

$$\begin{cases} w_{lo}^{L5}(I+1)=w_{lo}^{L5}(I)+\Delta w_{lo}^{L5} \\ \Delta w_{lo}^{L5}=-\mu_{lo}\frac{\partial(O.F)}{\partial w_{lo}^{L5}}=-\mu_{lo}.\frac{\partial(O.F)}{\partial y_o^{L5}(I)}.\frac{\partial y_o^{L5}(I)}{\partial w_{lo}^{L5}(I)}=\mu_{lo}.\sigma_o^{L5}.y_l^{L4}\end{cases} \tag{40}$$

In the following, we can provide two error indicators based on the propagation process in the 4th layer of the proposed algorithm. The layer 4 propagation error equations are:

$$\begin{cases} \sigma_l^{L4}=-\frac{\partial(O.F)}{\partial y_l^{L4}(I)}=-\left[\frac{\partial(O.F)}{\partial y_o^{L5}(I)}\right]\frac{\partial y_o^{L5}(I)}{\partial y_l^{4}(I)}=\sigma_o^{L5}.w_{lo}^{L5}(I) \\ \sigma_{jl}^{L4}=-\frac{\partial(O.F)}{\partial y_{jl}^{L4}(I)}=-\left[\frac{\partial(O.F)}{\partial y_o^{L5}(I)}.\frac{\partial y_o^{L5}(I)}{\partial y_l^{L4}(I)}\right]\frac{\partial y_l^{L4}(I)}{\partial y_{jl}^{L4}(I)}=\sigma_l^{L4}.y_z^{L3}(I)\end{cases} \tag{41}$$

The error index and normalized weight update based on the propagation process and learning rate in layer 3 are:

$$\sigma_k^{L3}=-\frac{\partial(O.F)}{\partial y_z^{L3}(I)}=-\left[\frac{\partial(O.F)}{\partial y_o^{L5}(I)}.\frac{\partial y_o^{L5}(I)}{\partial y_l^{L4}(I)}\right]\frac{\partial y_l^{L4}(I)}{\partial y_p^{L3}(I)}=\sigma_l^{L4}.y_{jl}^{L4}(I) \tag{42}$$

$$\begin{cases} w_{ik}^{L3}(I+1)=w_{ik}^{L3}(I)+\Delta w_{ik}^{L3} \\ \Delta w_{ik}^{L3}=-\mu_{ik}\frac{\partial(O.F)}{\partial w_{ik}^{L3}}=\begin{pmatrix}-\mu_{ik}.\frac{\partial(O.F)}{\partial y_o^{L5}(N)}.\frac{\partial y_o^{L5}(I)}{\partial y_l^{L4}(I)}.\frac{\partial y_l^{L4}(I)}{\partial y_p^{L3}(I)} \\ .\frac{\partial y_z^{L3}(I)}{\partial w_{ik}^{L3}(I)}\end{pmatrix}=\left(\mu_{ik}.\sigma_k^{L3}.W_{ik}^{L3}\right)\end{cases} \tag{43}$$

The error index and the update of the average value of the AGF based on the propagation process in layer 2 are:

$$\sigma_j^{L2}=\frac{\partial(O.F)}{\partial N_j^{L2}(I)}=\left(-\left[\frac{\partial(O.F)}{\partial y_{jl}^{L4}(I)}\right]\frac{\partial y_{jl}^{L4}(I)}{\partial y_j^{L2}(I)}.\frac{\partial y_j^{L2}(I)}{\partial N_j^{L2}(I)}\right)=\sum_{jl}\sigma_{jl}^{L4}y_{jl}^{L4}(I) \tag{44}$$

Table 1
MG specifications [8,34].

Parameters	Value
Nominal active power	1.4 MW
BESS energy (Nissan Altra lithium-ion battery)	230 kWh
Base power	1000 kW = 1pu
PV power (Chroma 62150H-6005)	110 kW
WT power	110 kW
Diesel generator power (SD500 | 15.2L |-GENERAC)	500 kW
Nominal MG voltage	V_{LL} = 400 V, V_{ph} = 220
Nominal MG frequency	50 Hz
Line impedance per kilometer (XLPE Cable)	$Z_{feeder1} = 0.521 + j0.083$ $Z_{feeder2} = 0.395 + j0.078$ $Z_{feeder3} = 0.442 + j0.088$
Converter THD	THD < 5 %
Power factor	$0.85 \le Cos\varphi \le 0.95$
Charge and discharge efficiency	0.95

$$\Delta M_j^{L2} = -\mu_M \frac{\partial(O.F)}{\partial M_j^{L2}} = -\mu_M \left[\frac{\partial(O.F)}{\partial N_j^2(N)}\right] \frac{\partial N_j^{L2}(N)}{\partial M_j^{L2}(N)}$$
$$= \begin{cases} \dfrac{(2\mu_M \sigma_j^{L2}).(x_i^{L2} - M_j^{L2})^2}{(d_{left-j}^{L2})^2} & -\infty < x_i^{L2} < M_j \\ \dfrac{(2\mu_M \sigma_j^{L2}).(x_i^{L2} - M_j^{L2})^2}{(d_{right-j}^{L2})^2} & M_j < x_i^{L2} < +\infty \end{cases} \quad (45)$$

The equations for updating the left and right standard deviation of the AGF are:

$$\Delta d_{left-j}^{L2} = \left(-\mu_{left-d} \frac{\partial(O.F)}{\partial d_{left-j}^{L2}} = -\mu_{left-d} \left[\frac{\partial(O.F)}{\partial N_j^{L2}(I)}\right] \frac{\partial N_j^{L2}(I)}{\partial d_{left-j}^{L2}(I)}\right)$$
$$= \left(-\frac{(2\mu_{left-d} \sigma_j^{L2}).(x_i^{L2} - M_j^{L2})^2}{(d_{left-j}^{L2})^3} \middle| \begin{array}{c} M_j^{L2}(I+1) = M_j^{L2}(I) + \Delta M_j^{L2} \\ d_{left-j}^{L2}(I+1) = d_{left-j}^{L2}(I) + \Delta d_{left-j}^{L2} \\ d_{right-j}^{L2}(I+1) = d_{right-j}^{L2}(I) + \Delta d_{right-j}^{L2} \end{array} \right) \quad (46)$$

$$\Delta d_{right-j}^{L2} = \left(-\mu_{right-d} \frac{\partial(O.F)}{\partial d_{right-j}^{L2}} = -\mu_{right-d} \left[\frac{\partial(O.F)}{\partial N_j^{L2}(I)}\right] \frac{\partial N_j^{L2}(I)}{\partial d_{right-j}^{L2}(I)}\right)$$
$$= \left(-\frac{(2\mu_{right-d} \sigma_j^{L2}).(x_i^{L2} - M_j^{L2})^2}{(d_{right-j}^{L2})^3} \middle| \begin{array}{c} M_j^{L2}(I+1) = M_j^{L2}(I) + \Delta M_j^{L2} \\ d_{left-j}^{L2}(I+1) = d_{left-j}^{L2}(I) + \Delta d_{left-j}^{L2} \\ d_{right-j}^{L2}(I+1) = d_{right-j}^{L2}(I) + \Delta d_{right-j}^{L2} \end{array} \right) \quad (47)$$

To increase the speed of the learning algorithm, it is possible to use the adaptive error factor, which is caused by the error of the prediction power and the instantaneous power compared to the reference values. Therefore, the adaptive error rules for active power, reactive power, V/F indicators are:

$$AdaptiveError \begin{cases} \sigma_{o-P}^5 = (P_{ref} - P_{ins}) + (\widehat{P}_{ref} - \widehat{P}_{ins}) = e_P + \widehat{e}_P \\ \sigma_{o-Q}^5 = (Q_{ref} - Q_{ins}) + (\widehat{Q}_{ref} - \widehat{Q}_{ins}) = e_Q + \widehat{e}_Q \\ \sigma_{o-V}^5 = (V_{ref} - V_{ins}) + (\widehat{V}_{ref} - \widehat{V}_{ins}) = e_V + \widehat{e}_V \\ \sigma_{o-f}^5 = (f_{ref} - f_{ins}) + (\widehat{f}_{ref} - \widehat{f}_{ins}) = e_f + \widehat{e}_f \end{cases} \quad (48)$$

To guarantee the learning algorithm and the efficiency of the suggested approach, discrete time Lyapunov function analysis has been used, and in this article, for brevity, the discrete time Lyapunov function analysis equations have been omitted [28,34]. To analyze the performance of the suggested approach, the absolute error integral index of each power system parameter can be used. The absolute error integral index for different parameters in transient time t are:

$$E^{\text{absolute}} = \int_0^t |e(t)| dt \quad (49)$$

The absolute error integral index expresses the error of the proposed controller's output response compared to the reference value at the transient time t. Also, the operation time of the V/F protection equipment based on the operating time are:

$$\begin{cases} T_{Operation} = \dfrac{k_1}{(V_r/f_r)^{k_2} - 1} \cdot \dfrac{T_m}{10} \Rightarrow \text{over voltage}/frequency \\ T_{Operation} = \dfrac{k_1}{1 - (V_r/f_r)^{k_2}} \cdot \dfrac{T_m}{10} \Rightarrow under \text{ voltage}/frequency \end{cases} \quad (50)$$

Fig. 6 (a, b) shows the control model of RES and BESS in the grid connection operation mode and islanded operation mode.

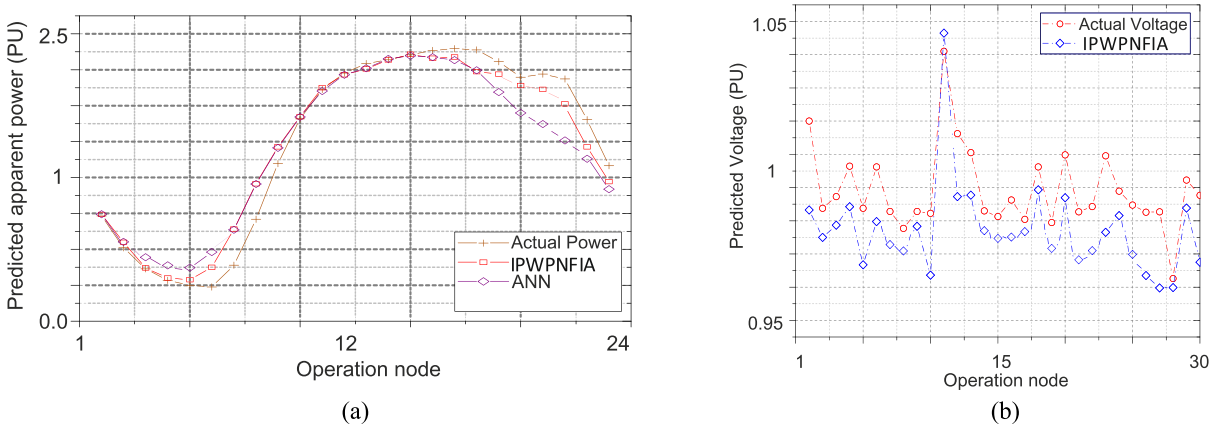

Fig. 7. The power and voltage prediction index at different operating points.

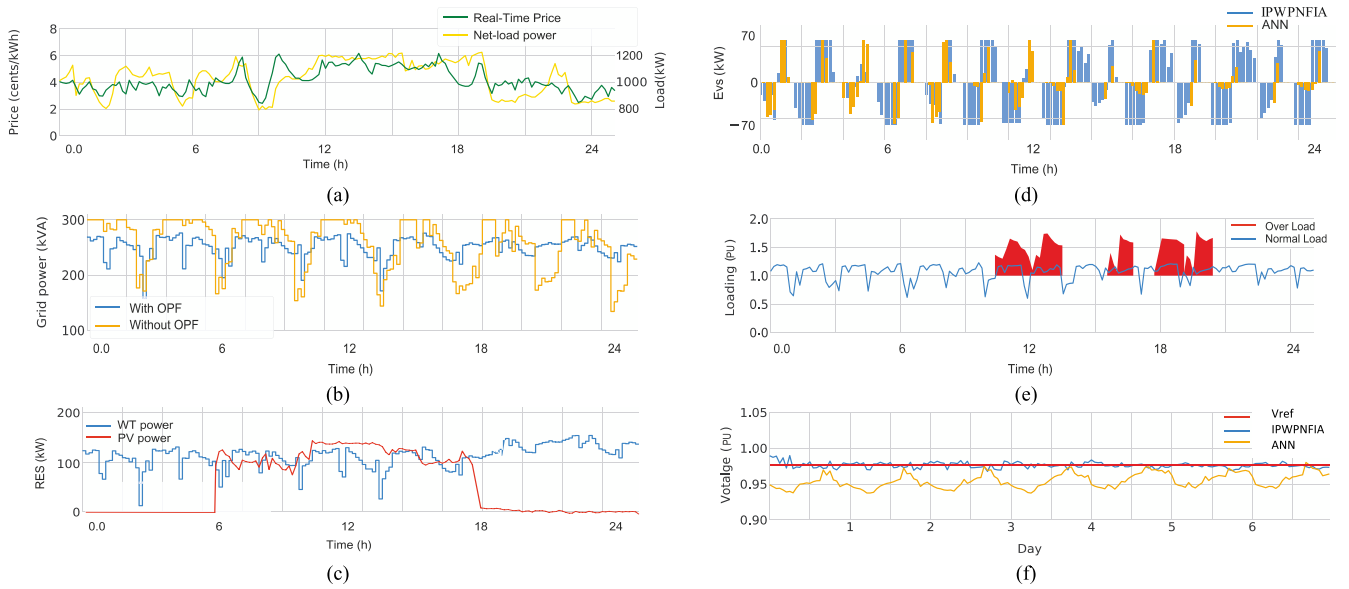

Fig. 8. Results of the scenario 1. (a) MG net power curve and spot price. (b) Main grid power exchange with the MG. (c) Power generation by the RES. (d) Charging and discharging of EV units based on DR programs and participation in MG power management. (e) Normal load and overload. (f) The MG weekly voltage profile.

5. Results, simulation and experimental setup

The proposed algorithm results are presented in 4 scenarios, which are:

Scenario 1: Investigation of the suggested approach in normal load operation and TOU-DRP algorithm execution

Scenario 2: Investigation of the suggested approach in the MG islanded operation and load oscillations.

Scenario 3: Investigation of the suggested approach in plug &play operating conditions.

Scenario 4: Investigation of the suggested approach in different uncertainties.

In addition to simulation results, experimental results are also presented in this section. Table 1 shows the characteristics of MG topology.

5.1. Scenario 1: Investigation of the suggested approach in normal loadnd developed DC microgrid energy operation and TOU-DRP algorithm execution

First, in this scenario, the power and voltage prediction based multiple and different operating points has been presented. The performance of the suggested approach in predicting and tracking the net power of MG is compared with the ANN [34] method and its results are presented in Fig. 7(a). According to Fig. 7(a), the suggested approach has predicted the MG net power with an error of approximately less than 1 %. The power prediction algorithm based on the IPWPNFIA method has been estimated at 24 operating points and the proposed algorithm has less tolerance than the ANN method. Also, according to Fig. 7(b), the voltage profile is predicted at 30 operating points and the IPWPNFIA method estimated the actual voltage with a tolerance of less than 1.1 %. In this scenario, the performance of the suggested approach has been analyzed under normal load conditions and the TOU-DRP algorithm execution. Fig. 8(a) shows the net power diagram of MG along with the real time price of the electric energy carrier. According to Fig. 8(a), the demand of subscribers has increased in the middle hours of the day. During these hours, part of the MG power is provided by the upstream grid. The MGCC calculates and sends control signals to each MGLC after implementing OPF and TOU-DRP algorithms in order to reduce operating cost and increase subscriber profit. For example, according to Fig. 8(b), the OPF results have been calculated and the required power of the MG is received from the upstream grid according to the OPF algorithm. Fig. 8(c) also shows the participation of the RES in providing MG power. As it is known, the WT units and PV panel combination show a suitable contribution in providing power. But as stated, the RES have uncertainty in power generation. Therefore, in the following scenarios, the performance of the IPWPNFIA method in controlling and managing the uncertainties of the RES is expressed. Fig. 8(d, e) show the performance comparison of the IPWPNFIA and the ANN methods for the optimal participation of EV units in the MG power supply, especially in critical conditions. According to Fig. 8(d), the negative powers indicate the discharge status of EV units and the positive powers indicate the charging status of EV units. Fig. 8(e) shows the MG operation curve in

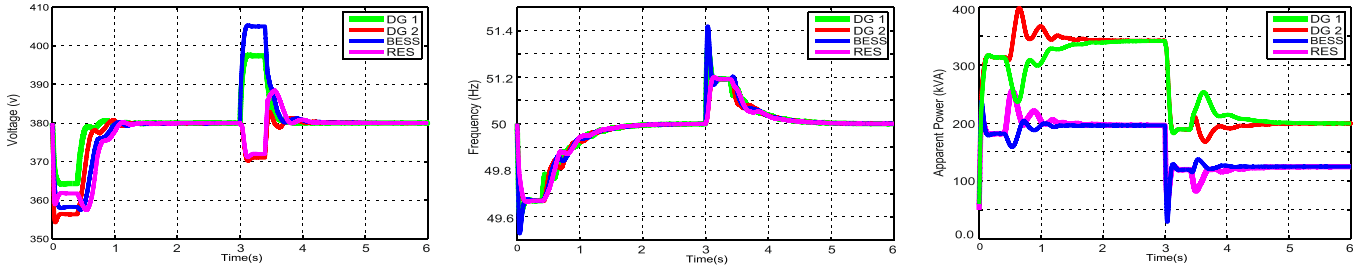

Fig. 9. The voltage, frequency and MG power in islanded mode and load fluctuations (scenario 2).

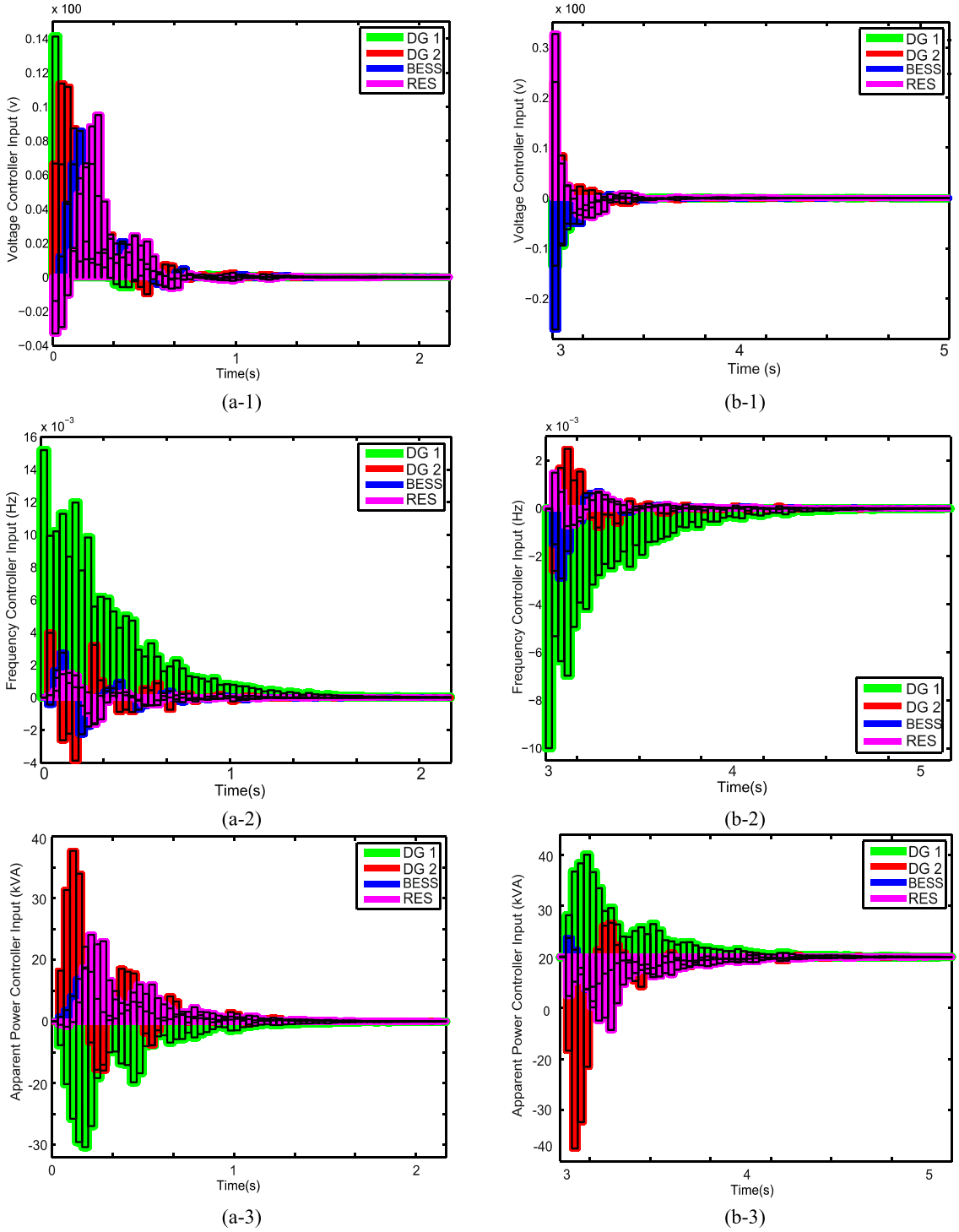

Fig. 10. Functions and input control signals to controllers based on scenario 2.

normal and overload loading. In several periods of time, the MG is overloaded. In this situation, BESS units (a part of BESS power belongs to EVs) have a suitable participation in providing the MG power and prevent buying power at a higher price. Therefore, the power stored in the battery of the EV units is injected into the MG in the periods when the price of the electric energy carrier has increased. According to the results, the performance of the suggested approach compared to the ANN method, in addition to high accuracy, also has a higher response speed. The use of the proposed platform, in addition to reducing operating costs, has also increased the profit of subscribers. Fig. 8(f) also presents the voltage profile during a week and at different loads. As it is clear from this figure, the IPWPNFIA follows the reference voltage with high accuracy and low tolerance, while the ANN method has a considerable error.

5.2. Scenario 2: Investigation of the suggested approach in the MG islanded operation and load oscillations

In this scenario, the suggested approach performance in controlling the MG power, V/F in the islanded operation and load fluctuations is

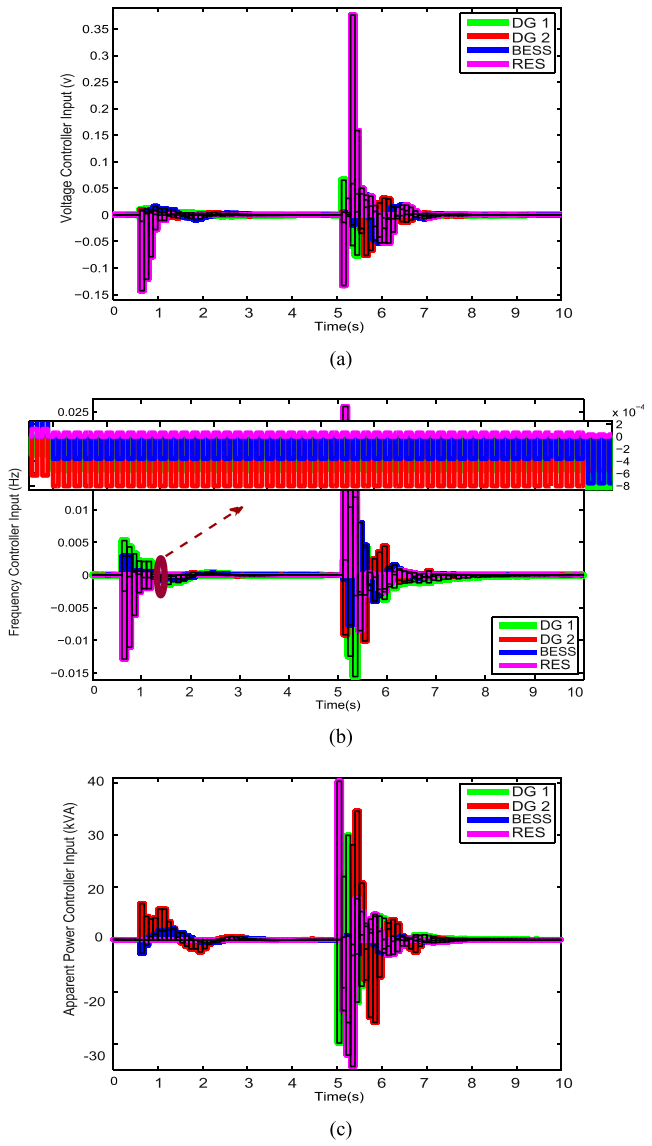

Fig. 12. Functions and input control signals to controllers based on scenario 3.

investigated and its results are presented. MG is separated from the main grid at t = 0sec and is operated in islanded mode. Transient conditions in power systems are divided into two categories: normal transient conditions (switching, load fluctuation, motor start-up, etc.) and unexpected transient conditions (lightning and short circuit). In normal transient conditions, protection units are programmed with a delay. While in unexpected transient conditions, protection units must act immediately to prevent damage to the power system. When the MG changes from grid-connected mode into the islanded mode, the power index changes greatly. Also, MG V/F experience critical transient conditions. In this situation, the probability of protection equipment activation will increase. If it is possible to control the critical transient conditions, frequent outages of the power system can be avoided, and in addition to controlling the MG stability, its operation can be ensured in safe conditions. In this scenario, when the MG switches to the islanded mode, the MGLC and related sensors provide signals of critical indicators such as the voltage, frequency, and net power of the MG to the MGCC. The MGCC determines the contribution of each unit in power supply by calculating the OPF and provides control signals to the MGLC.

According to Fig. 9(a, b), after the separation of MG from the main grid (t = 0 sec), in a short period of time and before the operation of protection units, the MG V/F index tend to the reference value of MG in

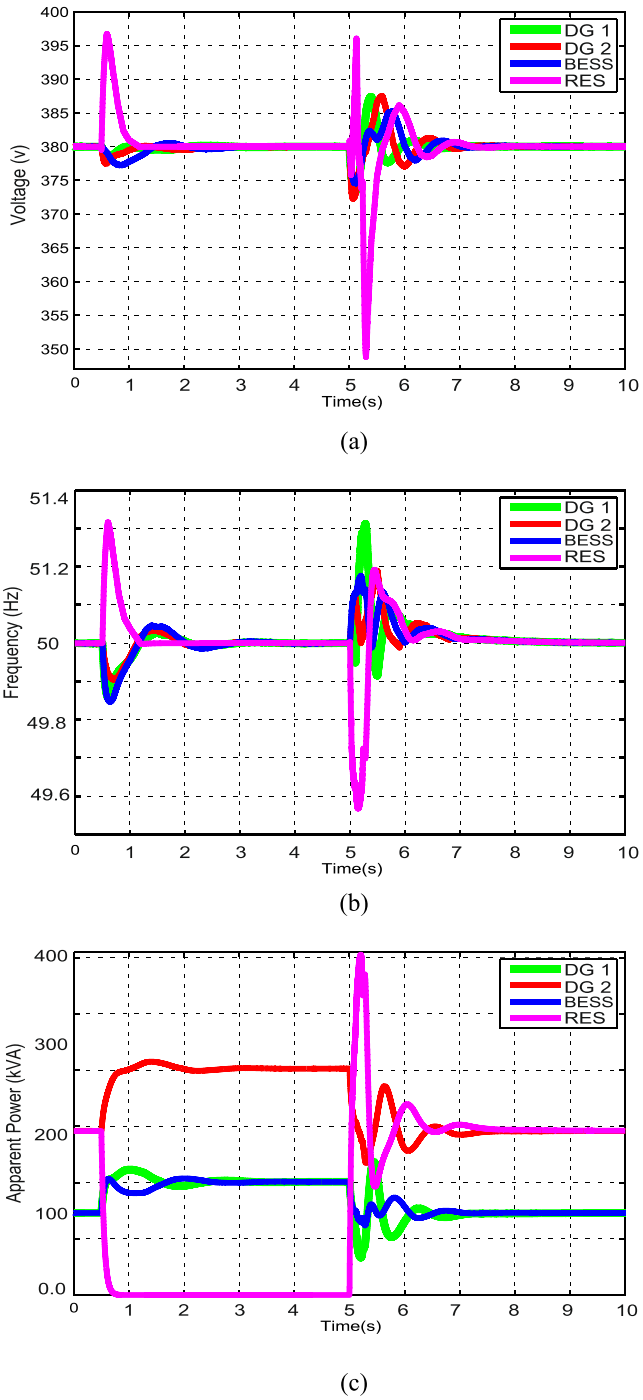

Fig. 11. MG voltage, frequency and power control in plug & play operating conditions (scenario 3).

addition to recovery. The conditions for following the reference values are programmed based on reducing the power, V/F deviation error from the reference values in the IPWPNFIA. According to Fig. 9(c), the contribution of different units in MG power supply is determined in islanded mode and each unit changes its power based on the MGCC and MGLC control signals. At t = 3sec, 15 % of the load is separated from the MG and causes power fluctuations as well as V/F fluctuations. In this situation, the MGCC sends new control signals to adjust and manage the power of different units. According to Fig. 9(c), the power of different units are reduced in order to control the V/F index, and the DG, BESS and RES units are stabilized at the new operating points. One of the important features of the IPWPNFIA is to reduce the voltage error from

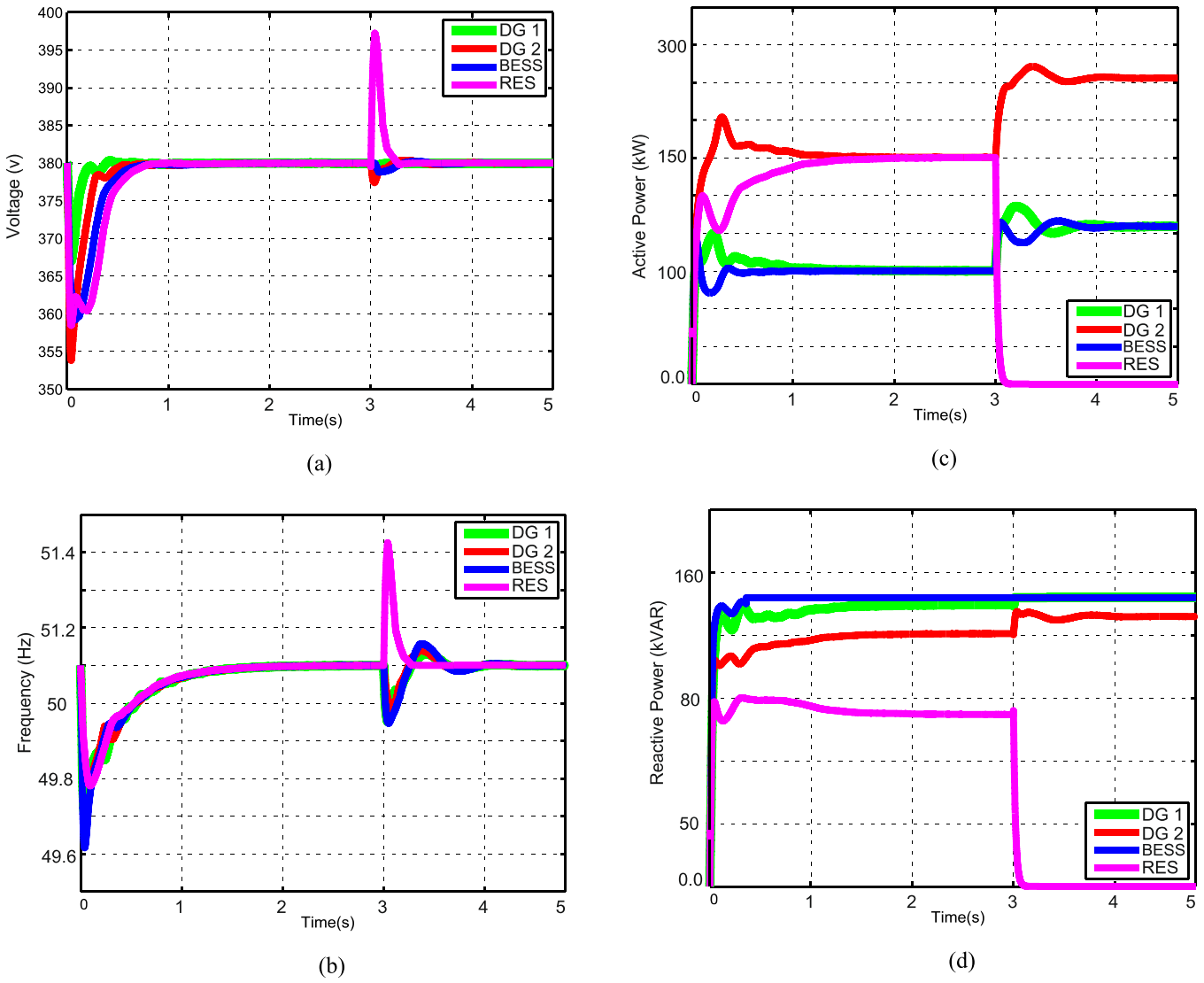

Fig. 13. The Voltage, frequency, active and reactive power control in plug & play operating conditions with load increase.

the reference value, which in turn provides a self-protection mechanism for DG units. If the voltage deviation is not compensated, it causes a circulating current between two diesel generator units and also prevents the proportional power sharing between the diesel generator units.

Fig. 10 shows the input data for the MG voltage, frequency and power controllers in islanded operating conditions and load fluctuations. According to Fig. 10 (a-1,2,3), functions and input control signals to MGLC are presented in order to control the voltage, frequency and power when the MG is separated from the main grid and operated in islanded mode. Fig. 10 (b-1,2,3) also shows the function signal and input control signals to the controllers in order to control the voltage, frequency and power in the condition of load fluctuations. Control signals based on error and deviation decrease of the voltage, frequency and power indicators from reference values are designed in the IPWPNFIA. It should be noted that the learning feature of the proposed algorithm, in addition to reducing the calculation time, also reduces the data estimation error. Another point is to improve the performance time of the suggested approach in order to coordinate with the protection units. The proposed algorithm manages the MG normal transient conditions in a way that does not require the unnecessary operation of protection units, and in addition to increasing the MG efficiency, it has also increased the reliability of MG operation.

5.3. Scenario 3: Investigation of the suggested approach in plug &Play operating conditions

In this scenario, the suggested approach capability in managing plug & play operating conditions is analyzed and its results are presented. In this scenario, the RES uncertainty is taken into consideration as plug & play operating conditions. At t = 0.5sec, RES units are disconnected from the MG and reconnected to the MG at t = 5sec. According to Fig. 11 (a, b, and c), after RESs disconnection from the MG, the MGCC calculates new control algorithms based on optimal power sharing between different DG and BESS units and sends them to MGLC. After the RES disconnection, the power of other units increases in order to control the V/F index. Therefore, by using the suggested approach, critical transient conditions are controlled and managed with proper accuracy and speed. According to Fig. 11 (a, b, and c), after the RES units reconnection, the MG again experiences critical transient conditions. In this situation, the MGCC calculates new control algorithms based on optimal power sharing between different units and sends them to MGLC. Therefore, the power of different units is reduced in order to reduce the deviation of the V/F index from the reference values. Considering that the MGCC is updated every 5 ms, the MGCC information is updated every second equivalent to 200 times and therefore changes in the MG topology can be monitored. Fig. 12 (a, b, and c) also shows the functions and control

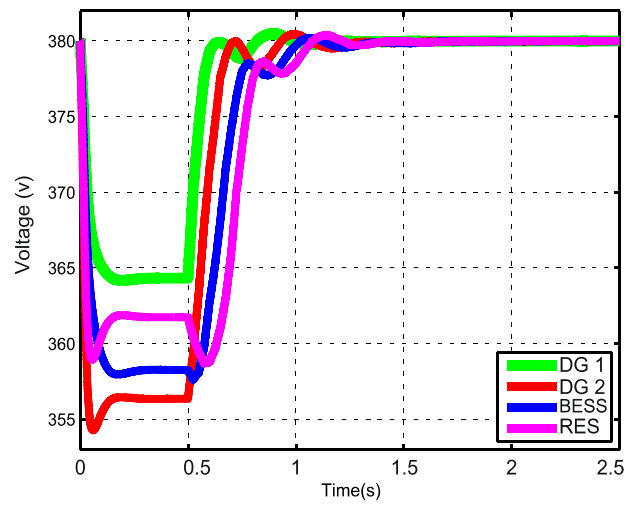

(a-1)

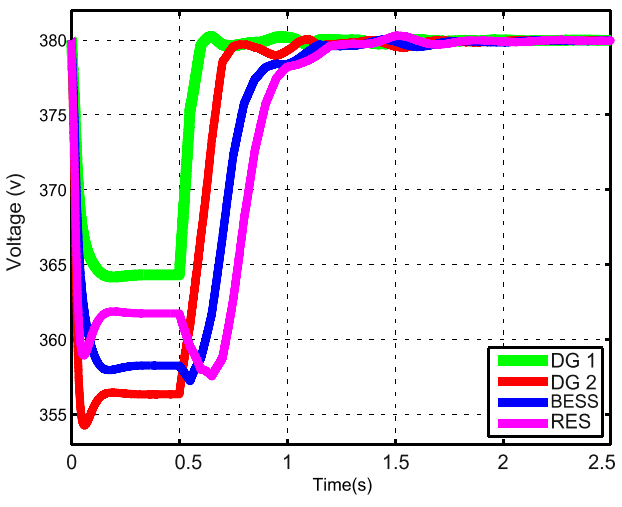

(b-1)

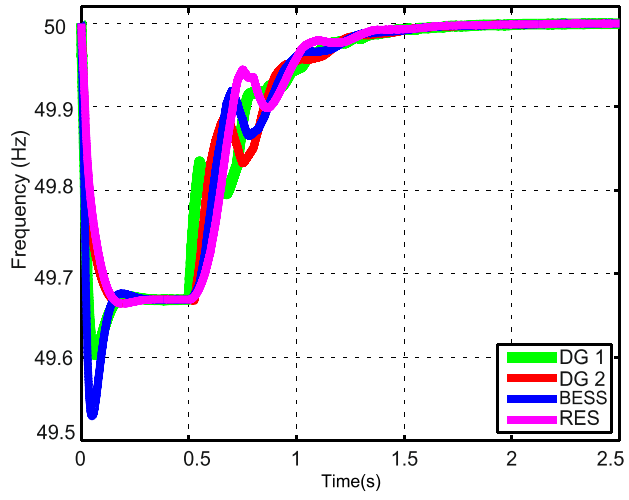

(a-2)

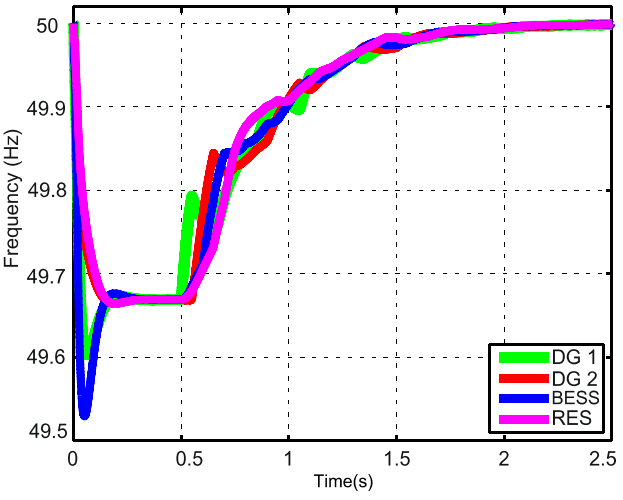

(b-2)

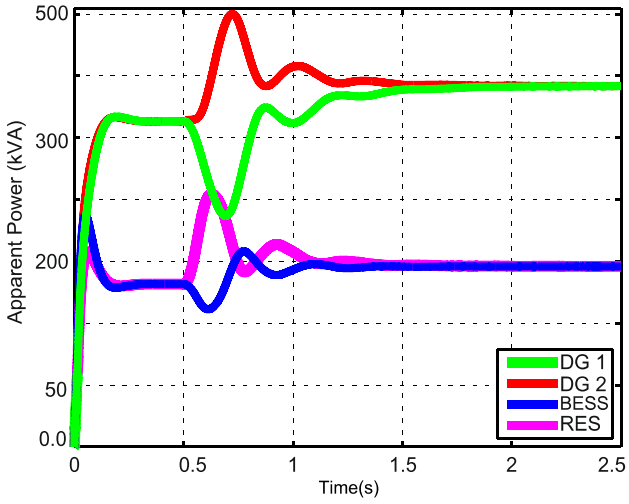

(a-3)

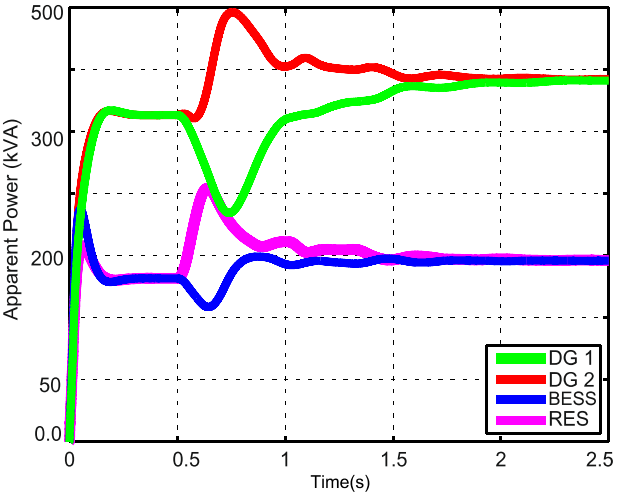

(b-3)

Fig. 14. The MG voltage, frequency and power control based on scenario 4. (a) Uncertainty index equivalent to $\chi = 10$. (b) Uncertainty index equivalent to $\chi = 20$.

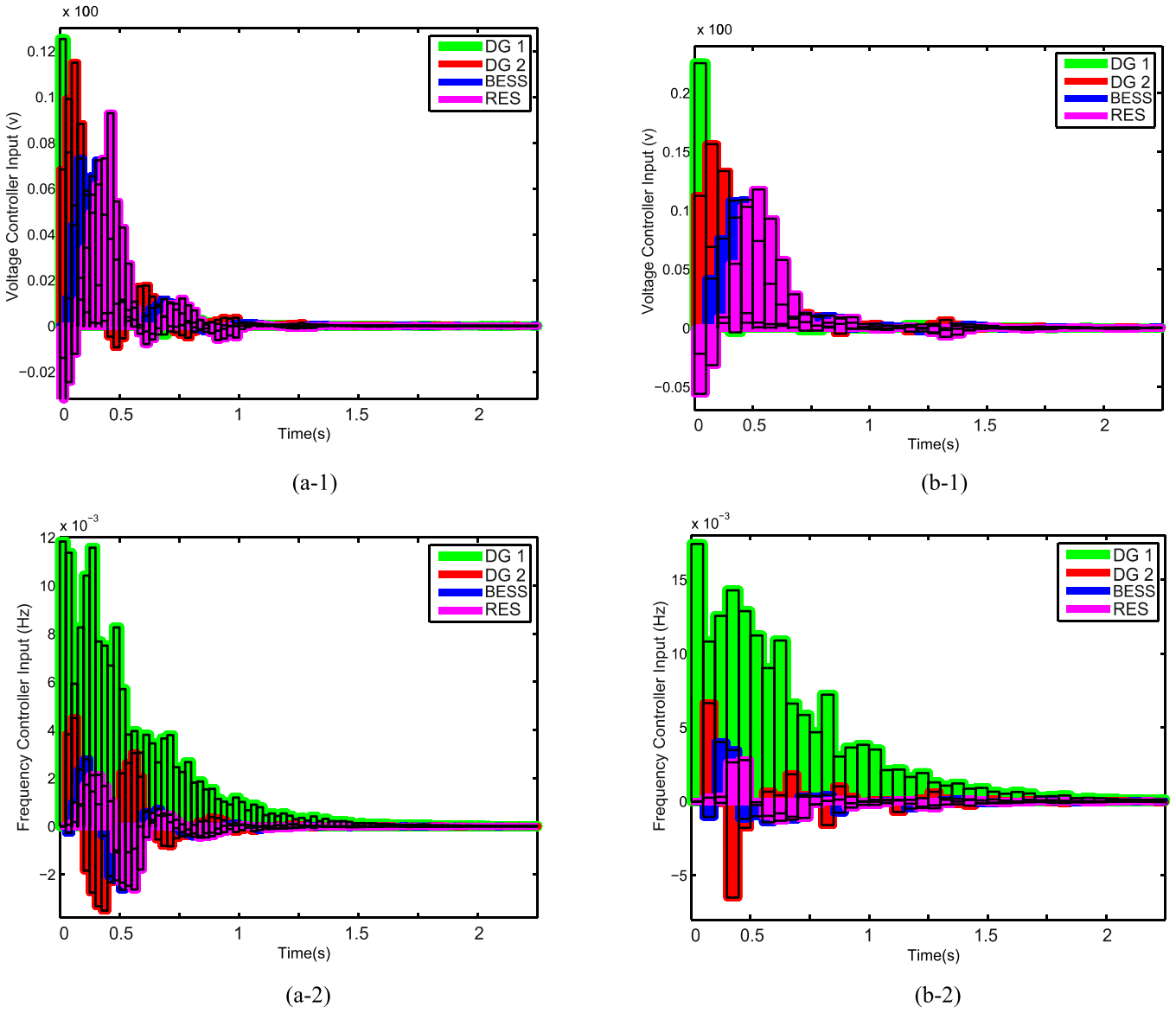

Fig. 15. Controller inputs based on scenario 4. (a) Uncertainty index equivalent to $\chi = 10$. (b) Uncertainty index equivalent to $\chi = 20$.

signals input to the MGLC in order to control the voltage, frequency, and power when the MG is in plug & play operation. As it is clear from Fig. 12, the deviation error of power, V/F indicators is controlled in a fraction of a second and avoids the unnecessary protection units operation. Fig. 13 also shows the plug & play operation along with load increase. MG is separated from the main grid at t = 0sec, and the IPWPNFIA, in addition to controlling the V/F indicators, also calculates and sends the proportional division of active and reactive power between other units. At t = 3sec, RES units are separated from the MG and MG load increases by 10 %. The MGCC based on the IPWPNFIA sends control signals to the MGLC and in addition to control the V/F index, it provides proportional power sharing management between DG and BESS units [35]. Therefore, in addition to controlling plug & play operating conditions, the proposed algorithm also shows the suitable stability in the increased load condition.

5.4. Scenario 4: Investigation of the suggested approach in different uncertainties

In this scenario, the performance of the suggested approach is presented in different ranges of uncertainty. In this scenario, the index of total uncertainties is considered equal to $\chi = 30$. The range between 0 and 20 includes normal transient uncertainties and the range between 20 and 30 includes unexpected transient uncertainties. As mentioned, the suggested approach is modeled in order to control the MG in normal transient conditions and prevent the unnecessary operation of the protection units. According to Fig. 14, MG is separated from the main grid at t = 0sec and is operated with an uncertainty index equal to $\chi = 10$ in islanded mode. According to Fig. 14 (a-1, 2, 3), the proposed algorithm in the time interval from 0 to 0.8 s, in addition to controlling the MG's V/F index, also provides proportional power sharing management between different power supply units.

If the uncertainty index of MG increases to $\chi = 20$, according to Fig. 14 (b-1, 2, and 3), the control of the V/F indicators will be done again by the proposed controller, but the time period for controlling these indicators will increase. Therefore, the presented results show the efficiency and robustness of the proposed algorithm in the conditions of increasing uncertainty indices. Fig. 15 also shows the inputs of the controllers based on the uncertainty index equal to $\chi = 10$ and $\chi = 20$.

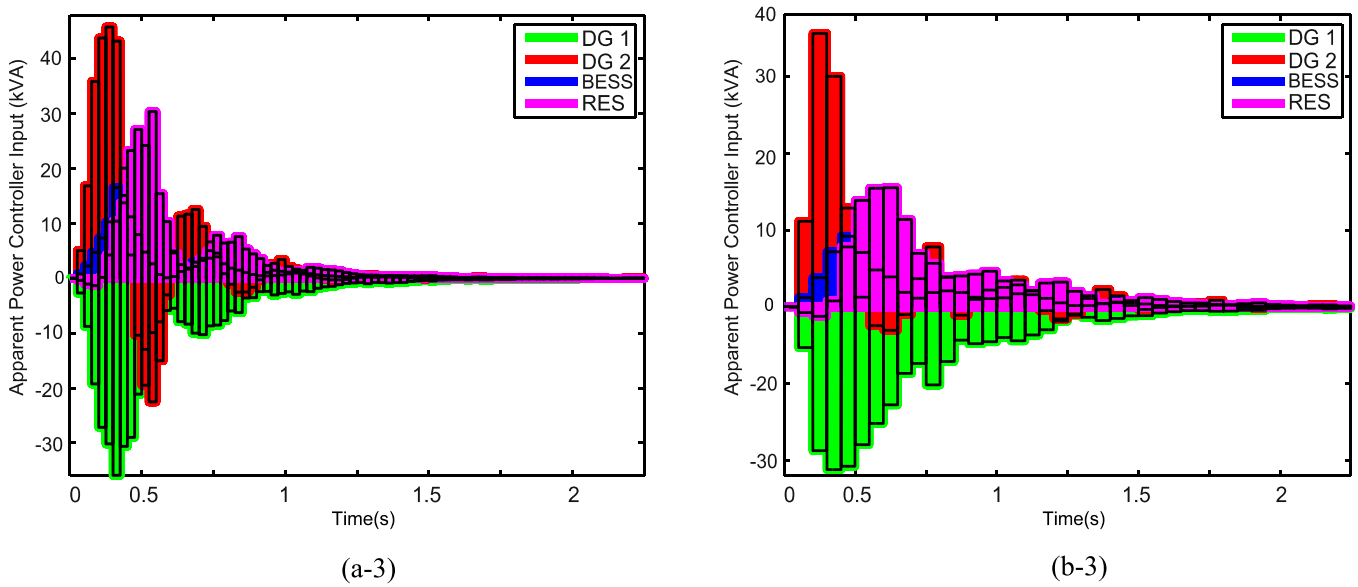

Fig. 15. (*continued*).

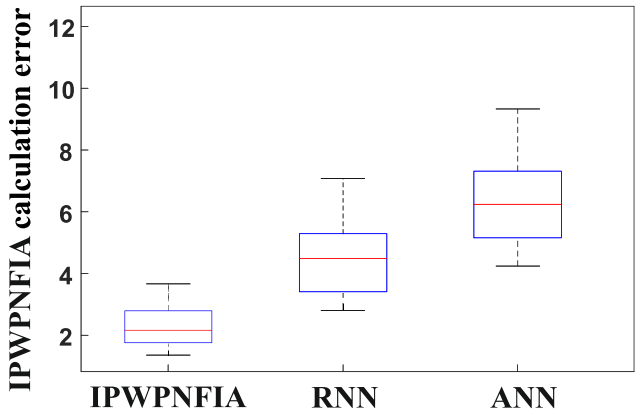

Fig. 16. Comparison of the computation error of the proposed approach with other methods.

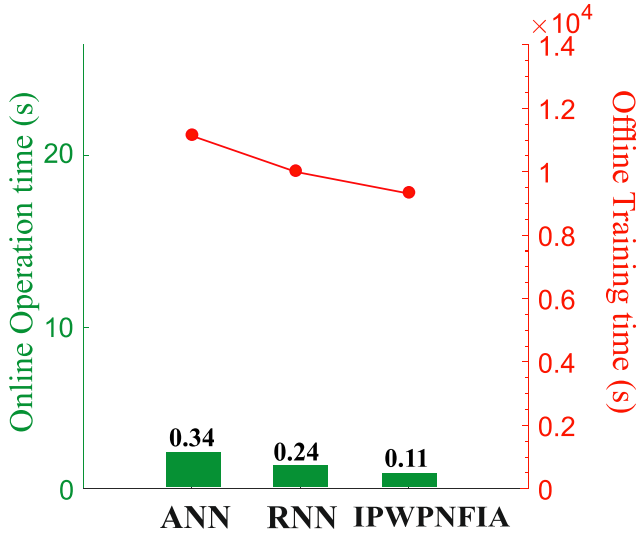

Fig. 17. Comparison of offline training and online operation computation time of the proposed approach with other methods.

5.5. *Experimental setup and results based on real time control and monitoring*

In this section, the experimental set-up using rapid control prototyping of the MG (RCP-MG) platform and the use of MATLAB/Simulink and RT-LAB software infrastructure as well as hardware infrastructure such as OPAL-RT hardware (OP5600 and OP8660) and Lab-Volt Electromechanical Training System is designed and presented. The experimental set-up has been programmed using TMS320F28335 digital signal processing (DSP) devices to monitor control signals. The proposed structure is implemented in MATLAB/Simulink software R2019b and two industrial computers with Intel®Core™ i7-7600U, 3.4 GHz CPU, and 16.00 GB RAM. The OP5600 equipment as real-time digital simulator and OP8660 equipment as hardware-in-the-loop (HIL) controller and data acquisition interface provide the control and monitoring environment of the suggested approach. OP8660 equipment creates a suitable structure for RT-LAB software communication with OP5600 equipment and other MG parts. RT-LAB software is also a real-time software that has the ability to implement RCPA based on hardware infrastructures such as OP5600 and OP8660.

The experimental setup model is presented in four categories, which are:

1. Modeling and simulation environment (this environment includes coding algorithms in MATLAB/Simulink and RT-LAB software along with the main server, MGCC and RCPA structure.
2. Real-time monitoring and control environment (this environment includes hardware equipment such as OPAL-RT hardware (OP5600 and OP8660) and LabVolt Electromechanical Training System.
3. Experimental setup environment (This environment includes MG hardware equipment such as photovoltaic panel, wind turbine modeling, converters, filters and storages.).
4. Measurement equipment environment and results recording (This environment includes various measurement equipment such as oscilloscope, AMI meters, vide o wall for MG monitoring and multimeters.

The IPWPNFIA model and The Online Back-propagation Learning Algorithm have a multi-level structure that makes it possible to avoid unnecessary and repetitive episodes and to perform processing operations in a shorter time. Therefore, this multi-level structure, in addition to reducing the computation burden and time, also reduces the memory

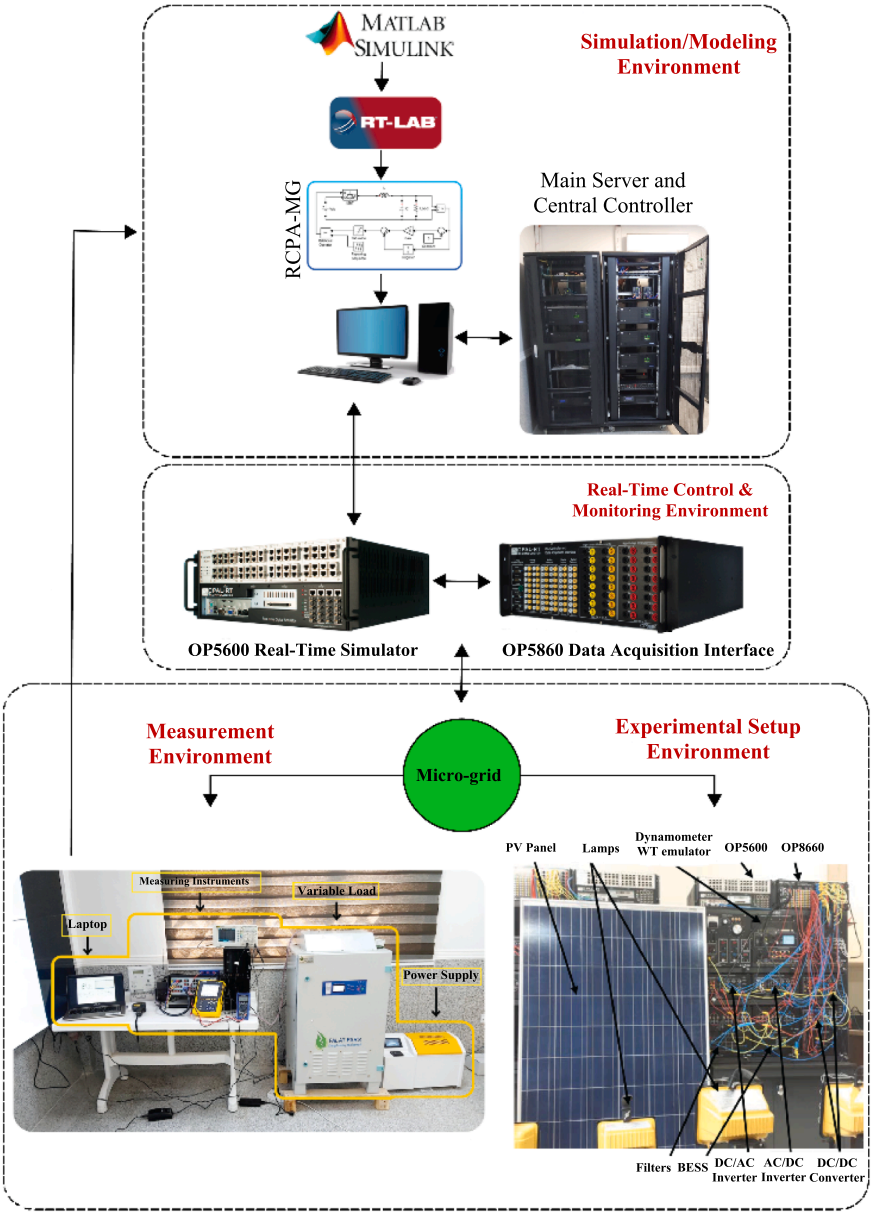

Fig. 18. Experimental setup and execution environments.

capacity and processing operations and turns the serial processing operations into parallel processing operations to avoid unnecessary and repetitive processes. Therefore, to better understand, the comparison of computation error and time of the proposed approach is presented with other methods. Fig. 16 shows the comparison of the computation error of the proposed approach with the RNN and ANN methods. According to Fig. 16, the computation error of the proposed approach is about 2 %, while the computation error of the RNN method is 5 % and the ANN method is 6 %. The significant decrease of the computation error based on the proposed approach compared to other methods is considered to be another prominent feature of the suggested approach. According to Fig. 17, the comparison of computation time in the structure of offline training and online operation is presented. The proposed approach not only benefits from less offline training time compared to other methods, but the operating time of the proposed approach also experiences a significant decrease compared to other methods. The proposed approach has not only reduced the computation time and burden but also reduced the memory capacity and time-consuming processing operations.

Fig. 18 shows the classification structure of the experimental set-up in four environments. Also, Fig. 19 shows the comparison of the experimental results and the simulation of V/F control on the load side, taking into account load decrease fluctuations and uncertainty caused by the communication system delay (200 *ms* and 400 *ms*). Table 2 also shows the comparison of the suggested approach response time with other general and intelligent methods. According to Table 2, the suggested approach response time is less than the protection unit pick-up time (the pick-up time of V/F protection equipment is 0.3–0.4 sec). While the ANN and RNN controller response time are the same as the protection equipment pick-up time, and therefore the performance interference between the protection units and the ANN and RNN controllers occur. The PID method response time is also more than the protection equipment pick-up time, and therefore the operation interference of the protection equipment and the PID controller occurs and the network faces frequent outages. Table 2 also shows the experimental

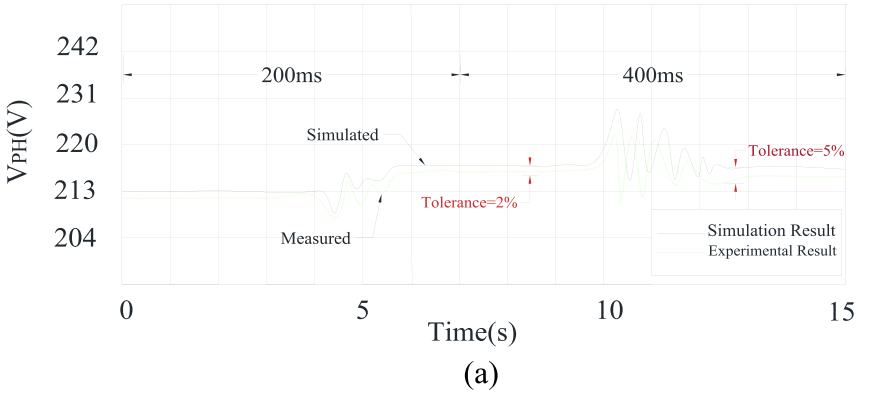

(a)

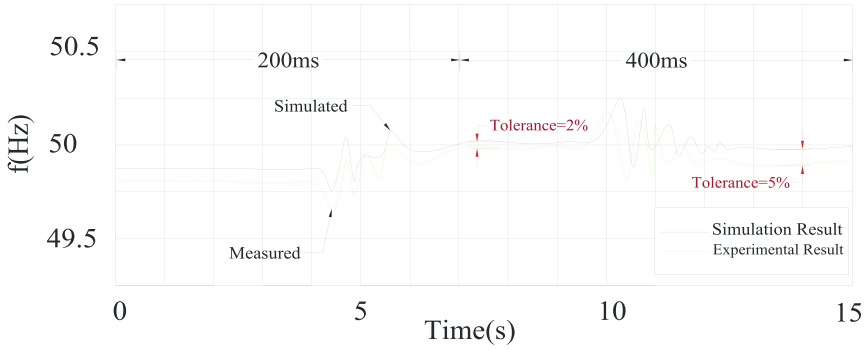

(b)

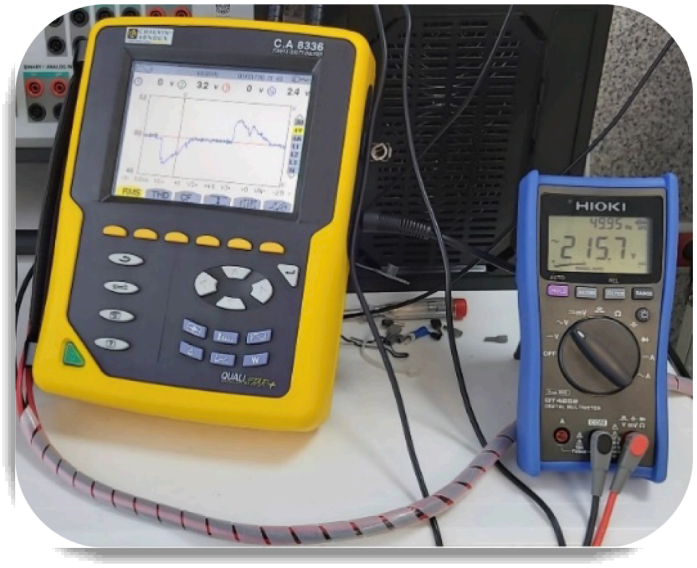

(c)

Fig. 19. Experimental results. (a) Load side voltage. (b) MG frequency. (c) Measurement environment results.

Table 2
Comparison of the suggested approach response time with other methods and comparison of the V/F deviation in switching conditions (grid connection to islanded mode).

Controller	Response Time (s)	V/F Deviation
PID	0.45	25v/0.5 Hz
ANN	0.34	19v/0.4 Hz
RNN	0.24	16.5v/0.38 Hz
IPWPNFIA	0.11	12v/0.099 Hz

results of V/F deviation index in different controllers. Considering that the voltage changes range is equal to 5 % of the rated voltage and the frequency changes range is equal to 1 % of the rated frequency, the suggested approach efficiency can be seen in the V/F index controller. The proposed controller has controlled the V/F index in the permissible range, while the ANN controller has controlled the voltage index in the critical range, and this condition increases the probability of protection equipment pick-up time. The PID controller has also controlled the voltage outside the standard range and the frequency in the critical range. Therefore, the interference of protection equipment and PID

controller causes frequent interruptions in the power system.

6. Conclusion

This study proposed a power management and control platform aiming to control the V/F metric of MGs in smart cities based on the IPWPNFIA considering RES, BESS, and various uncertainties. The suggested approach is implemented at the central and local controller levels. Since MG uses different equipment with linear/non-linear or probabilistic features, various uncertainties affect MG operations. The study scheduled the MGLC based on prototyping and implementing day-ahead power prediction algorithms. MGLC's power prediction results are provided to MGCC through the communication system. The MGCC also performs OPF computations according to MGLC data and reloads the control results to the MGLC. The proposed control platform considers the TOU-DRP metric to manage the BESS operation, which includes the EV batteries, to control the power and, consequently, V/F of the MG. Since the subscribers are equipped with the AMI based on the GPRS protocol, the TOU-DRP algorithm could be executed in the proposed grid. The TOU-DRP algorithm is executed based on the price elasticity theory.

The IPWPNFIA controller model is mainly based on data prediction and probability indicators. Therefore, it can be used probability tools such as probability functions with normal distribution and their generalized types to model the RES and EV uncertainties and significantly minimize prediction errors. The decrease in data prediction error makes the proposed algorithm more precise and reduces the computing time. Since the suggested approach is rule and knowledge-based, the IPWPNFIA controller minimizes the number of fuzzy function rules to reduce the computing time by taking advantage of the previous data-based training capability. V/F metric control is developed to avoid unnecessary activation of protection equipment under normal transient conditions.

The IPWPNFIA model and The Online Back-propagation Learning Algorithm have a multi-level structure that makes it possible to avoid unnecessary and repetitive episodes and to perform processing operations in a shorter time. Therefore, this multi-level structure, in addition to reducing the computation burden and time, also reduces calculation errors, memory capacity, and time-consuming processing operations. According to the results obtained from comparing the calculation error of the proposed approach with the RNN and ANN methods, the calculation error of the proposed approach is about 2 %, while the calculation error of the RNN method is equal to 5 % and the ANN method is equal to 6 %. A significant decrease in the calculation error based on the proposed approach compared to other methods is considered one of the prominent features of the suggested approach. Also, the results of comparing the response time of the proposed approach with the RNN and ANN methods show that the dynamic response speed of the proposed approach is 54.16 % higher than the RNN method and 67.64 % higher than the ANN method. Therefore, the obtained results show a high dynamic speed, a decrease in calculation time and burden, as well as a significant decrease in processing operations.

Since the suggested approach is implemented in a portion of the electrical energy distribution grid of Rajaee Port in Iran (a real small-scale MG), the performance of the suggested approach and IPWPNFIA controller is verified through different scenarios, the experimental results are presented, and the performance is also compared with other general and intelligent methods, e.g., PID and ANN. The experimental setup was designed and proposed using the RCP-MG platform, MATLAB/Simulink and RT-LAB software, and hardware infrastructures, e.g., OPAL-RT hardware (OP5600 and OP8660) Lab-Volt Electromechanical Training System. The results of this study confirmed the high performance of the proposed platform in the V/F control of MGs when faced with various uncertainties. The proposed platform had a high dynamic response speed and a short computing time.

This study's main challenge is analyzing the suggested approach based on intelligent data mining and machine learning algorithms to analyze big data and verify the suggested approach in large-scale grids.

CRediT authorship contribution statement

Reza Sepehrzad: Conceptualization, Methodology, Software, Investigation, Validation, Writing – original draft, Formal analysis, Supervision, Project administration. **Atefeh Hedayatnia:** Software, Investigation, Validation. **Mahdi Amohadi:** Writing – review & editing, Visualization, Investigation. **Javid Ghafourian:** Formal analysis, Visualization, Investigation. **Ahmed Al-Durra:** Supervision, Project administration, Investigation, Conceptualization, Methodology. **Amjad Anvari-Moghaddam:** Supervision, Project administration, Writing – review & editing.

Declaration of Competing Interest

The authors declare that they have no known competing financial interests or personal relationships that could have appeared to influence the work reported in this paper.

Data availability

Data will be made available on request.

Acknowledgments

This work was supported by Khalifa University of Science and Technology (KUST), Abu Dhabi, UAE, under Award CIRA-2021-063

References

[1] Mansouri SA, et al. A hierarchical scheduling framework for resilience enhancement of decentralized renewable-based microgrids considering proactive actions and mobile units. Renew Sustain Energy Rev 2022;168:112854.
[2] Ma Y, et al. Decentralized and coordinated scheduling model of interconnected multi-microgrid based on virtual energy storage. Int J Electr Power Energy Syst 2023;148:108990.
[3] Vahedipour-Dahraie M, et al. Short-term reliability and economic evaluation of resilient microgrids under incentive-based demand response programs. Int J Electr Power Energy Syst 2022;138:107918.
[4] Sepehrzad R, et al. Optimal energy management of distributed generation in microgrid to control the voltage and frequency based on PSO-adaptive virtual impedance method. Electr Pow Syst Res 2022;208:107881.
[5] Mansouri SA, et al. An interval-based nested optimization framework for deriving flexibility from smart buildings and electric vehicle fleets in the TSO-DSO coordination. Appl Energy 2023;341:121062.
[6] Mansouri SA, et al. An IoT-enabled hierarchical decentralized framework for multi-energy microgrids market management in the presence of smart prosumers using a deep learning-based forecaster. Appl Energy 2023;333:120560.
[7] Li Z, et al. A novel two-stage energy management of hybrid AC/DC microgrid considering frequency security constraints. Int J Electr Power Energy Syst 2023;146:108768.
[8] Sepehrzad R, et al. Intelligent energy management and multi-objective power distribution control in hybrid micro-grids based on the advanced fuzzy-PSO method. ISA Trans 2021;112:199–213.
[9] Muttaqi KM, Sutanto D. Adaptive and predictive energy management strategy for real-time optimal power dispatch from VPPs integrated with renewable energy and energy storage. IEEE Trans Ind Appl 2021;57(3):1958–72.
[10] Shan Y, et al. A unified model predictive voltage and current control for microgrids with distributed fuzzy cooperative secondary control. IEEE Trans Ind Inf 2021;17(12):8024–34.
[11] Abdolrasol MGM, et al. Artificial neural network based particle swarm optimization for microgrid optimal energy scheduling. IEEE Trans Power Electron 2021;36(11):12151–7.
[12] Xiong L, et al. A two-level energy management strategy for multi-microgrid systems with interval prediction and reinforcement learning. IEEE Trans Circuits Syst I Regul Pap 2022;69(4):1788–99.
[13] Zhao Z, et al. Distributed robust model predictive control-based energy management strategy for islanded multi-microgrids considering uncertainty. IEEE Trans Smart Grid 2022;13(3):2107–20.
[14] Qin Z, et al. Privacy preserving load control of residential microgrid via deep reinforcement learning. IEEE Trans Smart Grid 2021;12(5):4079–89.
[15] Hong T, et al. A bilevel voltage regulation operation for distribution systems with self-operated microgrids. IEEE Trans Smart Grid 2021;13(2):1238–48.

[16] Xia Y, et al. A safe policy learning-based method for decentralized and economic frequency control in isolated networked-microgrid systems. IEEE Trans Sustainable Energy 2022;13(4):1982–93.
[17] Yan R, et al. A multiagent quantum deep reinforcement learning method for distributed frequency control of islanded microgrids. IEEE Trans Control Network Syst 2022;9(4):1622–32.
[18] Li Y, et al. Optimal scheduling of integrated demand response-enabled community-integrated energy systems in uncertain environments. IEEE Trans Ind Appl 2021;58 (2):2640–51.
[19] Nazemi M, et al. Uncertainty-aware deployment of mobile energy storage systems for distribution grid resilience. IEEE Trans Smart Grid 2021;12(4):3200–14.
[20] Trujillo D, Torres EMG. Demand response due to the penetration of electric vehicles in a microgrid through stochastic optimization. IEEE Lat Am Trans 2022; 20(4):651–8.
[21] Lu X, et al. Optimal bidding strategy of demand response aggregator based on customers' responsiveness behaviors modeling under different incentives. IEEE Trans Ind Appl 2021;57(4):3329–40.
[22] Liu J, Singh R, Pal BC. Distribution system state estimation with high penetration of demand response enabled loads. IEEE Trans Power Syst 2021;36(4):3093–104.
[23] Aljohani TM, Ebrahim AF, Mohammed OA. Dynamic real-time pricing mechanism for electric vehicles charging considering optimal microgrids energy management system. IEEE Trans Ind Appl 2021;57(5):5372–81.
[24] Li Y, et al. Coordinating flexible demand response and renewable uncertainties for scheduling of community integrated energy systems with an electric vehicle charging station: A bi-level approach. IEEE Trans Sustainable Energy 2021;12(4): 2321–31.
[25] Cheng Y, et al. Low-carbon operation of multiple energy systems based on energy-carbon integrated prices. IEEE Trans Smart Grid 2019;11(2):1307–18.
[26] Bakhtiari H, Zhong J, Alvarez M. Predicting the stochastic behavior of uncertainty sources in planning a stand-alone renewable energy-based microgrid using Metropolis–coupled Markov chain Monte Carlo simulation. Appl Energy 2021;290: 116719.
[27] Fu L, et al. Electric vehicle charging scheduling control strategy for the large-scale scenario with non-cooperative game-based multi-agent reinforcement learning. Int J Electr Power Energy Syst 2023;153:109348.
[28] Sepehrzad R, et al. Islanded micro-grid frequency control based on the optimal-intelligent lyapunov algorithm considering power dynamic and communication uncertainties. Electr Pow Syst Res 2022;208:107917.
[29] Sepehrzad R, et al. An efficient multilevel interconnect control algorithm in AC/DC micro-grids using hybrid energy storage system. Electr Pow Syst Res 2021;191: 106869.
[30] Monfaredi F, Shayeghi H, Siano P. Multi-agent deep reinforcement learning-based optimal energy management for grid-connected multiple energy carrier microgrids. Int J Electr Power Energy Syst 2023;153:109292.
[31] Taheri S, Jooshaki M, Moeini-Aghtaie M. Long-term planning of integrated local energy systems using deep learning algorithms. Int J Electr Power Energy Syst 2021;129:106855.
[32] Lin X, Zeng S, Li X. Online correction predictive energy management strategy using the Q-learning based swarm optimization with fuzzy neural network. Energy 2021; 223:120071.
[33] Hassanzadeh ME, et al. Hierarchical optimal allocation of BESS using APT-FPSO based on stochastic programming model considering voltage sensitivity and eigenvalues analyses. Int J Electr Power Energy Syst 2023;153:109291.
[34] Sepehrzad R, et al. Intelligent hierarchical energy and power management to control the voltage and frequency of micro-grids based on power uncertainties and communication latency. Electr Pow Syst Res 2022;202:107567.
[35] Sepehrzad R, et al. Experimental and developed DC microgrid energy management integrated with battery energy storage based on multiple dynamic matrix model predictive control. Journal of Energy Storage 2023;74:109282.